17

BEAM SWITCHYARD DESIGN AND OPERATION

J. L. Harris, S. K. Howry,
E. J. Seppi, Editor, and H. A. Weidner

As previously discussed, the accelerator is capable of providing interlaced electron and/or positron beams at various pulse rates, currents, and energies. The beam switchyard (BSY) is designed to separate the various beams coming from the accelerator and deliver them to the appropriate experimenters' locations. A beam transport system consisting of pulsed and direct current magnets channels the beam through the switchyard to the various experimental setups on a pulse-to-pulse basis. This transport system and the associated instrumentation provides momentum analysis and control of the high-power beams up to the points where they are dissipated in targets or beam dumps. Figure 5-25 shows the arrangement of the research structures and experimental setups; Fig. 5-2 is an aerial view of the research area. Accelerator beams are delivered to two shielded and physically separated buildings known as end stations A and B. These buildings are located in a large research area which is available for the erection of other permanent and temporary buildings containing bubble chambers, spark chambers, and counting equipment. Three spectrometers are available in end station A. The central C-beam system transports the accelerator beam to targets and dumps within the beam switchyard housing, providing secondary beams for a bubble chamber and other experimental equipment located in the central part of the research area. Present beam arrangements are capable of delivering electron, photon, positron, μ-particle, π-meson, and K-meson beams to various experimental setups.

Considerable flexibility has been provided in the BSY for future beams and experimental facilities. Figures 5-23 and 17-1 through 17-3 show the locations of the equipment and beams in the switchyard. Provisions have been made for future development of a gamma-ray beam which could operate parasitically off the A system. In addition, the tunnel configuration provides

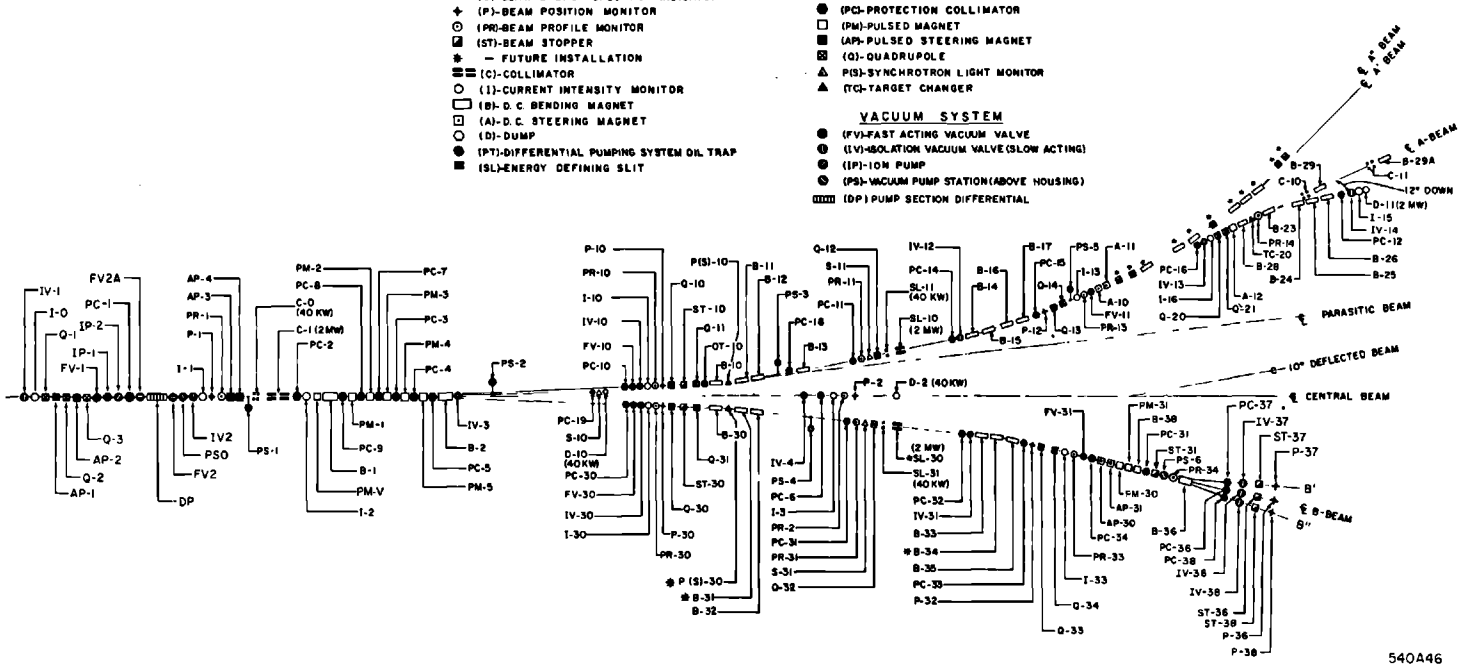

Figure 17-1 Schematic illustration showing the relative locations of magnets, energy absorbers, and beam instrumentation in the beam switchyard.

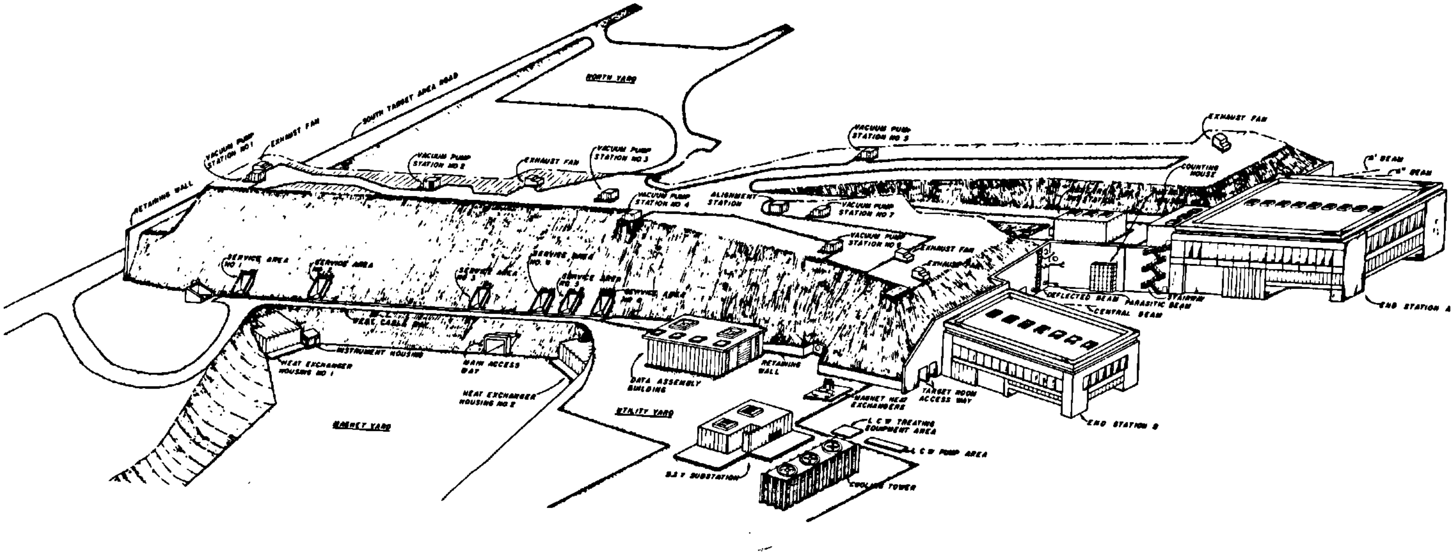

540-47-A

Figure 17-2 Isometric drawing of the beam switchyard area and end station building design.

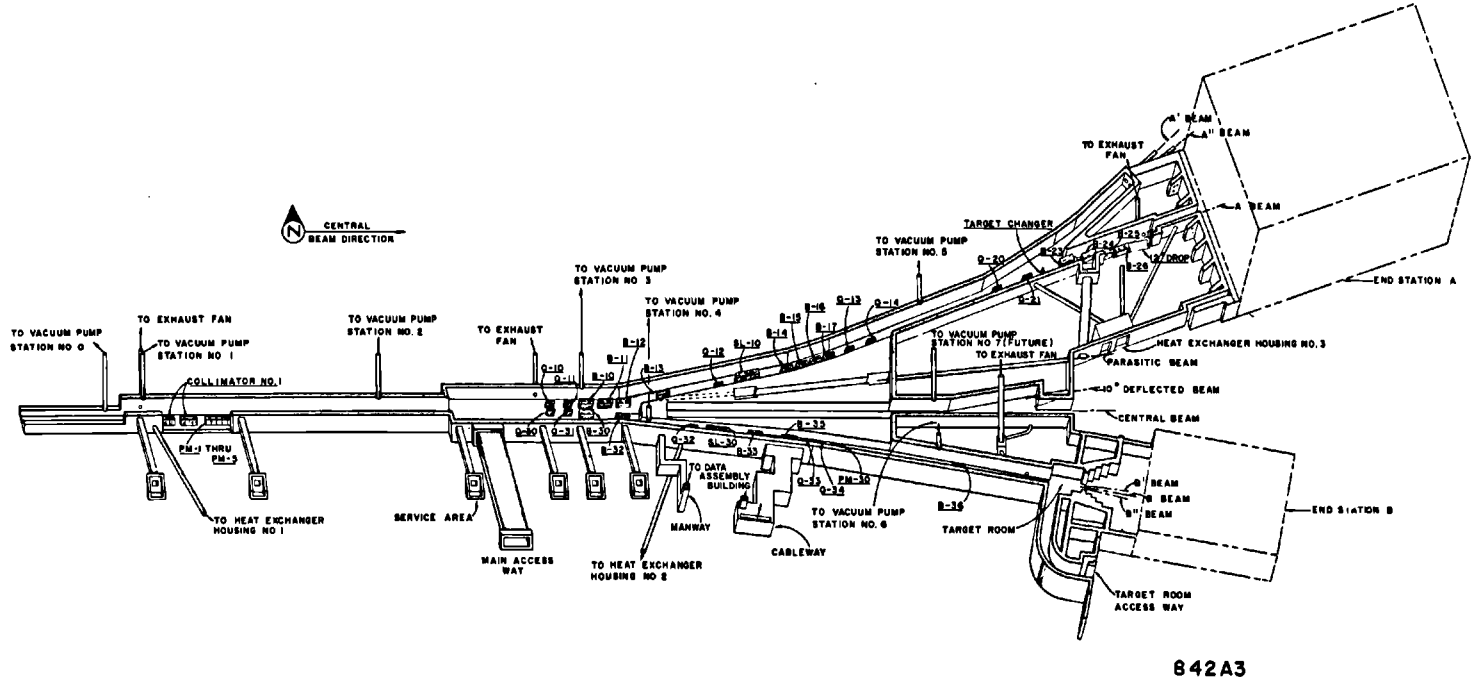

Figure 17-3 Isometric drawing of beam switchyard housing.

Table 17-1 Provisions for beam switchyard beams

Beam	*Status: July 1967*
Momentum analyzed electron or positron beam to end station A	Developed
A′ and A″ beams	Undeveloped
Momentum analyzed electron or positron beam to end station B with B-beam switching	Developed
Photon beam, end station A	Developed
Central beam	Being developed
10° deflected beam	Undeveloped
Parasitic beam	Undeveloped

for future beams (designated A′, A″) off the A system. Table 17-1 gives a list of arrangements which have been made for particle and photon beams from the beam switchyard. The table indicates the status and planned development of beams as of the fall of 1967.

The design of systems capable of handling the high beam power available from the accelerator and also using the accelerator's multiple beam flexibility presents numerous problems in instrumentation, mechanical design, and physical layout. The following discussion includes a description of the BSY, primary transport system and the optics of momentum analysis, an outline of the problems associated with the transport of high-intensity beams, a description of the beam switchyard design which was developed to solve these problems, and the results of BSY tests and early operation experience. Problems associated with BSY transport magnets and momentum calibration, instrumentation and control, beam energy absorbers, component alignment, and radiation shielding are discussed in Chapters 18, 19, 20, 22, and 26, respectively. Descriptions of the BSY vacuum system, cooling-water system, electrical system, and physical plant have been included in chapters covering these topics for the entire accelerator facility.

17-1 Beam switchyard transport and momentum analysis (SKH)

The magnets in the BSY and transport systems provide the deflection and focusing necessary to deliver momentum-analyzed beams to the A and B experimental areas. The essential optics of the systems were proposed by K. L. Brown.[1] System A was studied on a semiquantitative basis by Penner,[2] who concurred that it would be an acceptable system subject to more precise calculations. These two transport systems are illustrated in Figs. 17-1 and 5-23. The design criteria for systems A and B are summarized in Table 17-2. Since the A and B systems are nearly identical, only the transport system for beam A will be described. Methods of optimizing the A system and differences between the A and B systems will be described.

Table 17-2 Design characteristics of the beam switchyard transport systems A and B

Parameter	*System A*	*System B*
Momentum	The transport system will operate in the momentum range from below 1 GeV/c to 25 GeV/c.	The transport system will operate in the momentum range from below 1 GeV/c to 25 GeV/c. The system can easily be modified to operate up to 40 GeV/c.
Acceptance	The system will accept and pass without loss a beam with the following phase space: beam radius 0.3 cm, angular divergence 10^{-4} rad, momentum width up to 2.6% total. Actually, the accelerator provides an electron beam of considerably smaller phase space, but the positron beam has the above phase space.	The system will accept and pass without loss a beam with the following phase space: beam radius 0.3 cm. angular divergence 10^{-4} rad, momentum width up to 5.2% total.
Beam characteristics	The transport system is capable of handling 0.6 MW of beam power continuously. The pulse repetition rate is 0 to 360 pulses/sec, and the pulse width is 0.020–1.7μsec.	The transport system is capable of handling 0.1 MW of beam power.
Resolution	The transport system is capable of resolving $\pm$0.05% in momentum at the slit. The mean momentum of the beam is reproducible to $\pm$0.02%. The momentum width and mean momentum passed by the system is independent of the operation of the accelerator and the performance of the pulsed magnets.	The transport system is capable of resolving $\pm$0.1% in momentum at the slit. The mean momentum of the beam is reproducible to $\pm$0.05%. The momentum width and mean momentum passed by the system is independent of the operation of the accelerator and the performance of the pulsed magnets.
Momentum calibration	The absolute value of the mean momentum passing through the system is determined to $\pm$0.2%. The dispersion at the momentum defining slit is 0.15%/cm	The absolute value of the mean momentum passing through the system is determined to $\pm$0.5%. The disperion at the momentum defining slit is 0.3%/cm.
Achromaticity	The system is achromatic; that is, after leaving the last bending magnet, the momentum and transverse position distribution within the beam are uncorrelated.	The system is achromatic; that is, after leaving the last bending magnet, the momentum and transverse position distribution within the beam are uncorrelated.
Isochronism	After passing through the system, the longitudinal extent of the bunch does not exceed $\pm$20° RF phase (at 2856 MHz) for $\Delta P/P = \pm 1\%$; this is equivalent to a bunch length of $\pm$0.6 cm.	After passing through the system, the longitudinal extent of the bunch does not exceed $\pm$20° RF phase (at 2856 MHz) for $\Delta P/P = \pm 3\%$; this is equivalent to a bunch length of $\pm$0.6 cm.

The A and B transport systems

Functionally, the A transport system is characterized by the following features, which are illustrated in Fig. 17-1. The beam from the accelerator is directed through the collimator C-1 by the pulsed steering magnets AP 1-4. After its size and position have been determined by the collimator, its beam enters the pulsed magnets PM-1 through PM-5 and is deflected to the quadrupole doublet, Q-10, Q-11. For monoenergetic beams, the doublet Q-10, Q-11 forms images as follows: the beam cross section at the center of the pulsed magnet PMV is focused vertically to form an image in the horizontal axial plane at the symmetry quadrupole Q-12; the beam cross section at the center of the pulsed magnet group PM-1 through PM-5 is focused horizontally to form an image in the vertical axial plane at the front of the slit SL-10. The horizontal focus at the entrance to the slit optimizes the momentum resolution of the system. The bending magnets B-10 through B-13 disperse the beam horizontally for momentum resolution at the slit. Vertically, the symmetry quadrupole has little effect on the beam because of the small vertical size of the beam resulting from the vertical focus at the symmetry quadrupole. In the horizontal plane the symmetry quadrupole recombines the different momenta, so that after passing through the second set of bending magnets B-14 through B-17, the beam is achromatic. The quadrupole doublet, Q-13, Q-14, produces a low-divergence beam by imaging (approximately) the slit to infinity. The final beam then drifts to the end station without appreciable spreading. A small adjustment of the final location and direction of this beam can be made using the steering magnets A-10 and A-11.

Essentially, the transport system up to this point has maintained a constant phase volume. In the A-beam, a target, beam dump, and the associated magnets and instruments for generating a photon beam are located in the drift space following Q-20, Q-21. The pair of doublets (Q-13, Q-14 and Q-20, Q-21) can be used to achieve a desired spot size, or for phase-matching either the electron beam or, to some extent, the photon beam to experiments. The drift space following the latter doublet is chosen in conjunction with the focal length of the doublet to give the desired spot size or the proper phase match into the experiment or auxiliary system. At 15 meters from the doublet, an electron beam spot size of 1 mm is possible.

In the B-beam, after passing through the doublet Q-33, Q-34, which corresponds to Q-13, Q-14 in the A line, the beam is steered by two pulsed steering magnets, AP-30, AP-31, into two pulsed magnets PM-30 and PM-31, which can deflect the beam either left or right by 0.35° or let the beam pass undeflected. The beam then encounters the slit magnet B-36, which is actually two C-type deflecting magnets which perform the function of adding a further deflection of 1.7° to a beam deflected to the left or right by PM-30, PM-31. In addition, the properties of the C-type magnets are such that they will allow an undeflected incident beam to pass with no added deflection. Thus, the

B-beam can be provided in end station B along three different beam lines on a pulse-to pulse basis.

Selection of fixed parameters

Certain parameters of the transport systems were fixed at the outset by considerations not entirely optical. Compromises involving spatial clearance, magnet design, economy, and the like, fixed the criteria of the system. Each of the fixed parameters of the system will now be discussed. The total bending angle of the pulsed magnets PM-1 through PM-5 was set at 0.5°. The magnitude of this angle is optically not significant. The difficulties in designing a pulsed magnet system with the necessary stability and reliability at a reasonable cost, and of which the magnetic field can be programmed on a pulse-to-pulse basis, set the upper limit for the bending angle.

After passing through the pulsed switching magnets, the deflected beam must drift until it is sufficiently offset from the center line of the straight-ahead beam to allow insertion of the next magnets of the system, namely the Q-10, Q-11 doublet. Assuming the 0.5° deflection from the pulsed magnets above, a drift of 78.5 meters gives an offset of 70 cm (27.5 in.) which is sufficient. This drift distance D_1, essentially the distance from the source to the focusing quadrupole doublet Q-10, Q-11, is also important because it fixes the monochromatic beam image size at the slit. This image size determines the ultimate (or zero slit width) momentum resolution of the system. It should be small so that similar images of neighboring momenta do not overlap excessively. To a first approximation, the momentum range passing through a vanishingly small width slit in system A is

$$\frac{\Delta P}{P} \approx \frac{x_0}{D_1 \gamma} \tag{17-1}$$

where P is the momentum, γ is the total angle of bend of the first group of magnets B-10 through B-13, and x_0 is the horizontal extent of the beam spot at the collimator. For $\gamma = 12°$ (see below), $x_0 = 0.3$ cm, and $D_1 = 78.5$ meters, the ultimate resolution is roughly

$$\frac{\Delta P}{P} \approx 0.018\% \tag{17-2}$$

The bending magnets B-10 through B-13 serve a dual purpose, deflecting the beam so that the end stations can be physically separated, and dispersing it for momentum analysis. The angle of bend was fixed at 12° as a rather loose compromise between two conflicting requirements. The first was economic—increasing the bend angle decreases the overall cost of creating a given separation between the two end stations (although more magnets are needed, tunnel length is decreased). The second constraint was optical—the greater

the angle of bend, the greater the deterioration of beam isochronism. For a momentum band pass of $\pm 1\%$, a 24° bend increased the bunch spread by $\pm 15°$ in RF phase. This increase, when combined with the initial bunch length, makes the total bunch length spread near the limiting value of $\pm 20°$ (see Table 17-2). The bend is accomplished using identical 3-meter magnets, each bending 3°. Optically, they should be as close to the doublet, Q-10, Q-11, as possible in order to maximize the dispersion. A distance of 1.5 meters between magnets is sufficient for standard instrumentation. To provide for the parasitic gamma beam, the separation between the second and third magnets was increased to 2 meters to allow insertion of a thin radiator for gamma production. Moreover, the fourth magnet (B-13) was moved 9 meters downstream to create clearance between the gamma beam and the magnet. As a result, the resolution deteriorated about 0.5% from its ideal value for closely spaced magnets; this is an acceptable loss. The bend angle of the magnet group B-14 through B-17 was chosen equal to that of B-10 through B-13 because this leads to the smallest loss of isochronism in the beam. Also, this bend is necessary to separate the defined electron beam from the off-energy background radiation generated at the slit. The magnets B-14 through B-17 are also 3-meter long magnets and are spaced 1.5 meters apart.

The beam is dispersed in energy in traversing B-10 through B-13. The distance D_2 from the vertex of the bending group B-10 through B-13 to SL-10 is fixed by the momentum spread desired to pass through a fixed slit width. The distance was chosen to give a dispersion of 6 cm for a momentum spread of 1%.

Given the angle of bend for bending magnets and the distance D_2, then the distance D_3 from Q-12 to the doublet Q-13, Q-14 and the focal length of this doublet are fixed by the requirement that the emergent beam be made achromatic and dispersionless. The final determination of D_3 and the strength of the quadrupole setting will be discussed later. Another requirement on D_3 was that it had to be at least long enough to house the high-power slits SL-10 and SL-11 and associated equipment. The drift distance D_4 to the experimental end station was selected on the basis of giving the various experimental areas enough physical and radiological separation. Because the beam is made parallel in this region, there is no appreciable increase in beam size after drifting through the selected distance.

17-2 Quantitative determination of transport system parameters (SKH)

The detailed analysis of the beam switchyard transport system was performed by a general purpose digital computer program, TRANSPORT, which was developed at SLAC in 1962. It seems appropriate to outline in some detail the mathematical methods used in the program. Further details are to be found in Reference 3. A quantitative discussion of the parameters and specifications will also be given.

Beam transport analysis

The following notation has been adopted in discussing the differential beam coordinates of a particle with respect to the central ray of the transport system. The quantities x and θ refer to the differential position and divergence, respectively, in the horizontal (axial) plane. The quantities y and ϕ refer to the vertical plane. The variable z is the differential path length from the center of a particle bunch. The quantity $\delta = \Delta p/p$ is the differential momentum of the particle with respect to the momentum of a particle in the central ray. The transformation equation for the six differential coordinates of a particle in passing from one point, $\mathbf{X}_0$, in the transport system to another, $\mathbf{X}$, can be written

$$\mathbf{X} = R\mathbf{X}_0 \tag{17-3}$$

or

$$\begin{pmatrix} x \\ \theta \\ y \\ \phi \\ z \\ \delta \end{pmatrix} = \begin{pmatrix} (x\,|\,x_0) & (x\,|\,\theta_0) & 0 & 0 & 0 & (x\,|\,\delta_0) \\ (\theta\,|\,x_0) & (\theta\,|\,\theta_0) & 0 & 0 & 0 & (\theta\,|\,\delta_0) \\ 0 & 0 & (y\,|\,y_0) & (y\,|\,y_0) & 0 & 0 \\ 0 & 0 & (\phi\,|\,y_0) & (\phi\,|\,\phi_0) & 0 & 0 \\ (z\,|\,x_0) & (z\,|\,\theta_0) & 0 & 0 & 1 & (z\,|\,\delta_0) \\ 0 & 0 & 0 & 0 & 0 & 1 \end{pmatrix} \begin{pmatrix} x_0 \\ \theta_0 \\ y_0 \\ \phi_0 \\ z_0 \\ \delta_0 \end{pmatrix} \tag{17-4}$$

The matrix R in the above equation is called the transformation matrix. The zeros which have been placed in the matrix depend on some rather general assumptions about the transport systems which will not be discussed here.

Transformation matrices for quadrupoles, bending magnets, and other fields are found in the literature.[1,2,3] For example, in a field-free region the matrix for a drift section of length L is

$$D = \begin{bmatrix} 1 & L & & & & \\ & 1 & & & & \\ & & 1 & L & & \\ & & & 1 & & \\ & & & & 1 & \\ & & & & & 1 \end{bmatrix} \tag{17-5}$$

The transformation matrix through an entire system is found by successive multiplication of individual matrices. It is now possible to formulate mathematically what is meant by the image of a source. Any particle leaving the source plane with a given displacement x_0 will arrive at the image plane with the displacement x regardless of the divergence θ_0, i.e., x is independent of θ_0, or $(x\,|\,\theta_0) = 0$.

The other optical conditions also translate into transformation matrix constraints:

1 Point-to-point horizontal image requires $(x \mid \theta_0) = 0$
2 Point-to-point vertical image requires $(y \mid \phi_0) = 0$
3 Horizontal image from infinity requires $(x \mid x_0) = 0$
4 Vertical image from infinity requires $(y \mid y_0) = 0$
5 Achromatic beam (horizontal) requires $(x \mid \delta_0) = 0$
6 Dispersionless beam (horizontal) requires $(\theta \mid \delta_0) = 0$.

These are a few special cases of constraints on the transformation matrix R. This matrix clearly depends on values of parameters such as drift region lengths, dipole strengths, and quadrupole gradients of elements making up the system. The computer program, TRANSPORT, solves the general problem of varying these parameters to find numerical solutions, if any, to given sets of constraints applied to given systems.

The behavior of the envelope of a group of particles is important in the design of any system in that it fixes the apertures of all the magnet elements and vacuum pipes. Given that the six differential coordinates are necessary to describe a particle, a group of particles will occupy a certain volume in this six-dimensional phase space. An ellipsoid volume in this phase space is a reasonable approximation for particles in a beam distributed about some ideal particle. Such an ellipsoid may be represented as a quadratic form.

$$\sum_{i=1}^{6} \sum_{j=1}^{6} a_{ij} x_i x_j \leq 1 \tag{17-6}$$

where x_i for $i = 1$ through 6 denotes $(x_0, \theta_0, y_0, \phi_0, z_0, \delta_0)$, the differential coordinates represented by $\mathbf{X}_0$ in Eq. (17-3).

Equation (17-6) may be written in matrix notation

$$\mathbf{X}_0^{\dagger} \sigma_0^{-1} \mathbf{X}_0 \leq 1 \tag{17-7}$$

where the matrix σ_0^{-1} denotes the matrix elements a_{ij} and the dagger superscript denotes the transpose vector. The matrix σ_0 uniquely characterizes the ellipsoid and, hence, the beam of particles. For convenience in what follows, σ, with or without subscripts, will be referred to as the beam matrix. Two observations can be made which follow from the properties of the quadratic form defined by σ: (1) The volume of the six-dimensional ellipsoid defined by σ is $(16/3)\pi(\det \sigma)^{1/2}$—this is the "phase space" occupied by the beam; (2) σ is a real, positive-definite symmetric matrix.

As a particle passes through a system of magnets it undergoes a transformation given by Eq. (17-3). The transformation for the beam matrix is

$$\sigma = R \sigma_0 R^{\dagger} \tag{17-8}$$

This can be seen by substituting into Eq. (17-7) as follows:

$$\begin{aligned} \mathbf{X}_0^{\dagger} \sigma_0^{-1} \mathbf{X}_0 = \mathbf{X}_0^{\dagger} [R^{\dagger} (R^{\dagger})^{-1}] \sigma_0^{-1} [R^{-1} R] \mathbf{X}_0 &= (R\mathbf{X}_0)^{\dagger} (R \sigma_0 R^{\dagger})^{-1} (R\mathbf{X}_0) \\ &= \mathbf{X}^{\dagger} \sigma^{-1} \mathbf{X} \leq 1 \end{aligned} \tag{17-9}$$

This leads to the following principle: Given the beam entering a magnet system and given the transformation matrix of the system, the beam leaving the system may be readily obtained by the transformation of Eq. (17-8).

To examine the significance of these symbolic transformations, consider the two-dimensional (x, θ plane) representation of the beam matrix,

$$\sigma = \begin{pmatrix} \sigma_{11} & \sigma_{12} \\ \sigma_{12} & \sigma_{22} \end{pmatrix} \tag{17-10}$$

with (det σ) $= \varepsilon^2$. Then

$$\sigma^{-1} = \frac{1}{\varepsilon^2} \begin{pmatrix} \sigma_{22} & -\sigma_{12} \\ -\sigma_{12} & \sigma_{11} \end{pmatrix} \tag{17-11}$$

and the expansion of $x^\dagger \sigma^{-1} x$ becomes the equation of an ellipse,

$$\sigma_{22} x^2 - 2\sigma_{12} x\theta + \sigma_{11} \theta^2 = \varepsilon^2 \tag{17-12}$$

The coefficients of the ellipse and, hence, the elements of the σ matrix can be given an interpretation with the aid of Fig. 17-4. The square root of the diagonal elements gives the projection of the ellipse upon the coordinate axes and this is the extent of the beam in the various coordinates. The correlation between components depends upon the off-diagonal term. It is defined as

$$r_{12} = \frac{\sigma_{12}}{(\sigma_{11})^{1/2}(\sigma_{22})^{1/2}} \tag{17-13}$$

The correlation measures the tilt of the ellipse and the intersection of the ellipse with the coordinate axes. The area of the ellipse is π det σ. Because the determinant of a product is the product of the determinants, so long as (det R) $= 1$, the area is invariant under

$$\sigma = R\sigma_0 R^\dagger \tag{17-14}$$

This is essentially a statement of Liouville's theorem for the magnetostatic fields employed. In the (important) case that the ellipse is upright, the area becomes $\pi(\sigma_{11})^{1/2}(\sigma_{22})^{1/2} = \pi x\theta$, a more familiar measure of phase volume.

Figure 17-4 Beam ellipse.

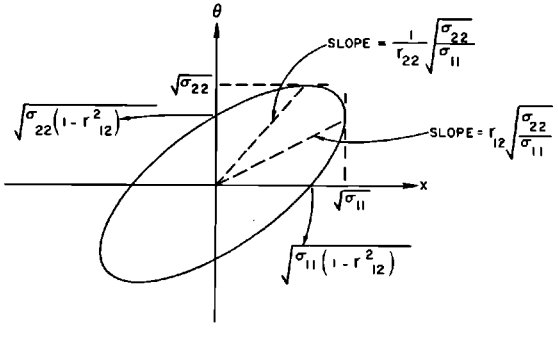

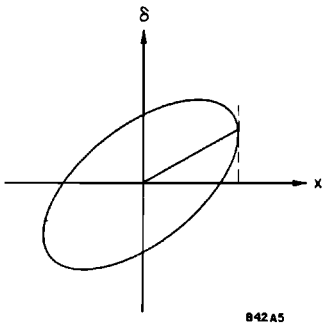

Figure 17-5 Projection of three-dimensional phase ellipsoid on x, δ plane.

The three-dimensional (x, 0, δ) extension of ray optics as published by Penner[2] requires a three-dimensional phase ellipsoid. Here again, in the units employed and for an upright ellipsoid, the volume of phase space becomes $\frac{4}{3}\pi x\, 0\delta$. The element σ_{13} defines the correlation between displacement and momentum and measures the *dispersion* in the beam. The projection of this ellipsoid on the x, δ plane is shown in Fig. 17-5. Thus, there obviously exists a correlation between particles with positive displacements and particles with positive momenta. This is the effect produced by deflecting the beam in a bending magnet.

Several other facets of the physical interpretation of the beam matrix warrant emphasis. The first point relates to the definition of the ellipsoid representing the beam. From the derivation of the transformation affecting the beam, it is apparent that particles cannot cross the surface of the ellipsoid. If their coordinates initially lie within the ellipsoid, they will remain within the ellipsoid through any number of linear transformations. This leads to a second point. The square roots of the diagonal elements indicate the maximum excursion of the particles in the beam from the reference trajectory. In particular, $(\sigma_{11})^{1/2}$ measures the horizontal extent of the beam. A plot of $(\sigma_{11})^{1/2}$ versus distance along the system is, therefore, the envelope of the beam and is the controlling factor in determining horizontal magnet apertures.

A characteristic of the beam envelope that becomes apparent upon plotting is the waist. This is a point where the horizontal (or vertical) extent of the beam is a minimum; in a field-free region it also happens to be a point where the ellipse is upright in the x, 0 plane, that is, $\sigma_{x\theta} = 0$ (see Fig. 17-6). At this point the beam is momentarily neither converging nor diverging. The fact that the minimum corresponds to an uncorrelated beam may be verified by determining the drift length that yields the minimum width,

$$\frac{\partial \sigma_{11}}{\partial L} = 0 \tag{17-15}$$

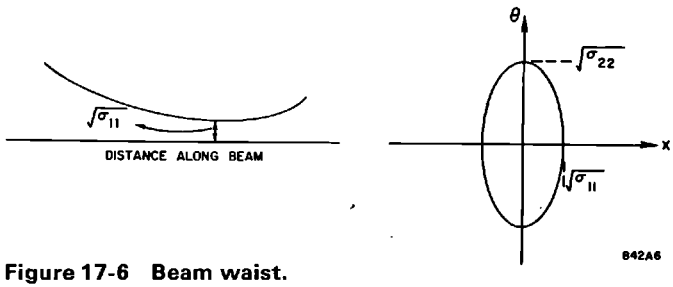

Figure 17-6 Beam waist.

The position of a waist depends upon the initial beam shape. However, it bears no useful relationship to the focal point of the magnets that may be used to produce the waist. For nonzero phase volumes, the location of a waist does not coincide with the location of a focus—that point at which the (x, θ) or (x, x) element of the transformation matrix vanishes. Evidently, if a small spot size at a target is desired, the target should be placed at a waist rather than a focus. The field-free drift distance to a waist is given by

$$L = -\frac{\sigma_{11}}{\sigma_{22}} = -r_{12}\left(\frac{\sigma_{11}}{\sigma_{22}}\right)^{1/2} \tag{17-16}$$

On the other hand, if L is a fixed distance from a quadrupole Q to a target, T, the optimum adjustment of Q to produce a small spot size at the target need not dictate a waist at the target, as Fig. 17-7 indicates.

Second-order effects

The previous paragraphs described a first-order model of beam optics. To establish, for a given beam transport system, the validity of approximations used in first-order theory, it is necessary to show that second-order aberrations for that system are negligible or at least sufficiently small. For this reason, a second-order beam optics model was developed and incorporated into

Figure 17-7 Effect of waist location on spot size.

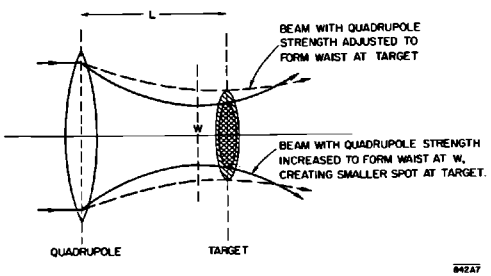

TRANSPORT. The approach is similar to the first-order case. One obtains a larger second-order transformation matrix for individual magnet types (e.g., bending magnet, quadrupole, sextupole), then combines them by matrix multiplication to get the second-order transformation of the system. Suppose that through a given magnet the transformation is

$$(x)_i = \sum_{l=1}^{6} R_{il} x_l + \sum_{l=1}^{6} \sum_{j=1}^{6} T_{ilj} x_l x_j + \cdots \tag{17-17}$$

The R_{il} form the first-order matrix described earlier. The T_{ilj} are the second-order coefficients of the transformation. For each individual magnet type, the T_{ilj} must be derived by expanding to second order the paraxial form of the general equations of motion of a charged particle through the magnet. Closed-form expressions for the T_{ilj} were obtained for various types of magnetic fields by different workers[1,4,5] and implemented into TRANSPORT. Then, with T available, a second-order transformation matrix through an individual magnet can be written. The product of such matrices, representing the magnets of the system in the appropriate order, yields the second-order transformation matrix of the entire system. The useful part of this matrix is the "T" partition. For example, the T_{236} element will give the effect on the final θ due to the product $(y_0\ \delta_0)$ of the initial ray. For this reason it is sometimes convenient to call T_{236} the $(\theta | y_0\ \delta_0)$ aberration. The reader is referred to Reference 1 for a complete discussion of second-order effects.

17-3 Optimization of system A (SKH)

In Section 17-1, the basic engineering criteria were given for the bending angles and drift distances D_1 and D_2. The remaining parameters of system A are the distance D_3 and the gradients of all five quadrupoles. The input acceptance requirements and other parameters fixed in the previous section together with certain constraints are used to determine values for these parameters. In practice, it is usual for a certain condition, e.g., a small beam cross section, to be required at some fixed position. The various conditions at different locations have been solved using the program TRANSPORT to yield a number of solutions to the beam design problem which have been collected to form a beam catalog.

The constraints which are common to almost all solutions are the following: (1) the transformation matrix element R_{12} from the center of the pulsed magnet group PM-1 through PM-5 to the front face of SL-10 is set equal to zero; (2) the matrix element R_{34} from the vertical pulsed magnet to the back face of the quadrupole Q-12 is set equal to zero (these two conditions determine the settings for Q-10 and Q-11 with two solutions; either Q-10 focuses horizontally and Q-11 vertically or vice-versa; (3) the matrix elements R_{16} and R_{26} to a point after the final bend at B-17 are set equal to zero. The location of the point is unimportant because once equal to zero [see Eq. (17-5)], these matrix elements remain equal to zero as the beam passes through

drift sections and quadrupoles. (The conditions $R_{16} = R_{26} = 0$ are, respectively, the achromatic and dispersionless conditions and their solution is essentially the same for all problems. These conditions determine the strength of Q-12 and the ratio of D_3 to D_2.)

To get a desired beam condition at a given distance D_4, the appropriate constraints are entered at that distance. The constraints may be for a waist ($\sigma_{12} = \sigma_{34} = 0$) or for a focus ($R_{12} = R_{34} = 0$) or for a parallel beam ($\sigma_{22} = \sigma_{44} = 0$) or perhaps for a given spot size such as ± 0.5-cm radius ($\sigma_{11} = \sigma_{33} = 0.5$). The parameters that are adjusted to fit these constraints are the gradients of the quadrupole doublet Q-13, Q-14 or of the doublet at Q-20, Q-21, the latter doublet being closer to the experimental area. Each of these may have either the focus–defocus or the defocus–focus order as in Q-10, Q-11. Between the choices of constraints and quadrupole order there are a large number of possible beam configurations. The beam catalog is simply a collection of some of these choices.

Second-order effects

There are two types of second-order aberrations—geometrical and physical. The two together make up the T_{ijk} array (previously discussed) for an individual magnet. The physical aberrations are the result of magnet imperfections, including the failure of first-order magnet parameters to describe adequately the magnetic field in the magnet. The geometrical aberrations are important when linear approximations are no longer valid. This occurs when any of the following conditions fail: $x/p \ll 1$; $y/p \ll 1$; $\theta \ll 1$; $\phi \ll 1$; $\delta \ll 1$.

For system A, $x/p \approx y/p \approx 10^{-3}$, $\theta \approx \phi \approx 10^{-4}$, and $\delta \approx 10^{-2}$. One would expect that if any second-order aberrations are important they would be chromatic in nature, namely, dependent on δ. However, because all second-order aberrations involve products of the above quantities, it is to be expected that second-order effects are negligible for the highly paraxial system A. This is, indeed, true except for bending magnet imperfections, and these alone will be discussed below. For a more detailed treatment, see Reference 6.

A dipole magnet with midplane symmetry has the following magnetic field components away from the fringe area:

$$\begin{aligned} H_z(x, y) &= 0 \\ H_y(x, y) &= H_0\left[1 - \frac{nx}{\rho} + \frac{\beta x^2}{\rho^2} + \left(\frac{n}{2} - \beta\right)\frac{y^2}{\rho^2} + \cdots\right] \\ H_x(x, y) &= H_0\left[-\frac{ny}{\rho} + \frac{2\beta xy}{\rho^2} + \cdots\right] \end{aligned} \tag{17-18}$$

where ρ is the radius of curvature of the reference trajectory in the magnet (for the 3° 3-meter magnets, $\rho = 57.296$ meters), H_0 is the field of the reference particle (at $x = 0$), n is the gradient or linear field index, and β is the quadratic

field index. The parameters H_0 and n are first-order field parameters. The quantity n can usually be made to vanish by symmetry of magnet design. Even if this is not the case, nonzero n effects can be countered by the gradients Q-10, Q-11. Since no term involving β in Eq. (17-18) is linear in the coordinates x and y, the first-order theory is independent of the value of β. If β is too large, differences between first-order theory and the actual field will appear. These differences will be seen in the second-order model.

There are three criteria for judging size and effect of second-order aberrations. They must not (1) affect the resolution of the system, (2) cause the beam to exceed magnet apertures, or (3) cause the minimum beam cross section at the target to be appreciably enlarged.

TRANSPORT second-order simulations on system A show that if the input beam divergence is $\approx 10^{-4}$, then noticeable second-order aberrations affecting resolution begin to appear for $|\beta| \approx 1500$. Also, the final beam cross section increases by a factor of 2 (over the $\beta = 0$ case) to 0.25 cm. This value of β determines the field homogeneity requirements.

The value of β for an actual magnet can be obtained from magnetic measurement data relating the field in the median plane $H_y(x, 0)$ to x, the horizontal displacement. The method by which such data are obtained is described below. These data may be fitted by least squares to a parabola,

$$H_{y(x,0)} = H_0\left(1 - n\frac{x}{\rho} + \frac{\beta x^2}{\rho^2}\right)$$

In this way estimates of β were calculated for all bending magnets. It was found that $|\beta| \leq 1600$ at all magnet currents. For magnet currents corresponding to momenta less than 20 GeV/c, $|\beta|$ is always less than 400. For $|\beta| \leq 400$, the quadratic field change at a distance of 1 cm from the reference trajectory on the median plane of the magnet is less than 2 parts in 10^5. The estimates of $|n|$ were in all cases less than 1 and were negligible.

The B transport system

The design philosophy for system B is identical to that for system A. The values of the design parameters are given in Table 17-2. The total angle of bend is 12.5°, derived from two 6° bends and a 0.5° deflection by the pulsed switching magnet. Magnets of the same design are used in both A and B systems. Two 3-meter magnets, each bending 3°, are used to obtain the 6° bend. The two magnets in each set are separated by 6 meters to allow the future insertion of a third magnet for expansion to the Stage II accelerator energy of 40 GeV/c. Each magnet then will bend only 2°. The effects of second-order aberrations are essentially the same as those for system A. The alignment criteria are also similar to those of the A system because the apertures in the second bending magnet group, as well as the reproducibility requirement on momentum definition, are equivalent to those of system A.

Alignment tolerances

The preceding discussion assumes that all the magnet axes coincide perfectly with the axis of the beam transport system. In practice this is not the case, so the mathematical model must be extended to deal with misalignments and to predict their effect on overall beam quality.

A rigid magnet has six degrees of freedom, three translational and three rotational. These are conveniently represented by six dependent quantities

$$\mathbf{m} = \begin{pmatrix} \delta x \\ \theta_x \\ \delta y \\ \theta_y \\ \delta z \\ \theta_z \end{pmatrix} \tag{17-19}$$

where δx, δy, δz are the displacements in the x, y, and z directions and θ_x, θ_y, θ_z are the rotations about the x, y, and z axes, respectively. The origin of the xyz coordinate system is taken as the magnet center, i.e., the point in a magnet of length L at which the reference particle has traversed length $L/2$. At that point the magnet axes coincide with the x, y, z components of the differential $\mathbf{X}$ vector discussed earlier. The vector $\mathbf{m}$ is a convenient quantity to use when discussing misalignment tolerances.

The problem is how to relate $\mathbf{m}$ to the transformation Eq. (17-3). When the magnet is misaligned, this becomes

$$\mathbf{X} - \mathbf{D} = R(\mathbf{X}_0 - \mathbf{D}_0) \tag{17-20}$$

The vectors $\mathbf{D}_0$ and $\mathbf{D}$ are the entrance and exit differential 6-vectors, respectively, of a ray traversing the path of the reference particle in a perfectly aligned magnet (see Fig. 17-8). Misalignment is a rigid transformation; therefore, the length and curvature of arc ACB are fixed and $\mathbf{D}$ and $\mathbf{D}_0$ are uniquely

Figure 17-8 Beam displacement due to magnet misalignment.

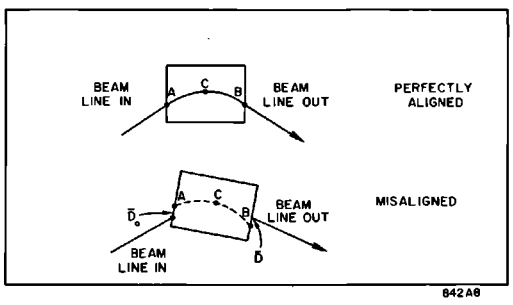

determined by **m**. For small |**m**| the relationship is

$$\begin{aligned} \mathbf{D}_0 &= A_0\,\mathbf{m} \\ \mathbf{D} &= A\mathbf{m} \end{aligned} \tag{17-21}$$

where

$$A = \begin{pmatrix} \cos\alpha & 0 & 0 & \rho\sin\alpha & \sin\alpha & 0 \\ 0 & 0 & 0 & 1 & 0 & 0 \\ 0 & -\rho\sin\alpha & 1 & 0 & 0 & -\rho(1-\cos\alpha) \\ 0 & -\cos\alpha & 0 & 0 & 0 & -\sin\alpha \\ -\sin\alpha & 0 & 0 & -\rho(1-\cos\alpha) & \cos\alpha & 0 \\ 0 & 0 & 0 & 0 & 0 & 0 \end{pmatrix} \tag{17-22}$$

and

$$A_0 = \begin{pmatrix} \cos\alpha & 0 & 0 & -\rho\sin\alpha & -\sin\alpha & 0 \\ 0 & 0 & 0 & 1 & 0 & 0 \\ 0 & +\rho\sin\alpha & 1 & 0 & 0 & -\rho(1-\cos\alpha) \\ 0 & -\cos\alpha & 0 & 0 & 0 & +\sin\alpha \\ +\sin\alpha & 0 & 0 & -\rho(1-\cos\alpha) & \cos\alpha & 0 \\ 0 & 0 & 0 & 0 & 0 & 0 \end{pmatrix} \tag{17-23}$$

α is one-half the angle of bend of the magnet, and ρ is the radius of curvature. For a quadrupole magnet, $\alpha = 0$ and $2\alpha\rho = L$, the magnet length, and the matrices reduce accordingly.

Substituting Eq. (17-21) into Eq. (17-20) gives a ray transformation through a magnet misaligned by **m**,

$$\mathbf{X} = RX_0 + (A - RA_0)\mathbf{m} \tag{17-24}$$

This completes the model for known misalignment **m**. Consider now an uncertainty in the magnet position and let the covariance matrix $\langle mm^\dagger \rangle$ measure the resulting distribution of magnet positions. If the position of the reference particle upon entering the magnet is $\langle xx^\dagger \rangle$ (due to, say, uncertainties introduced by misalignments of preceding magnets) and if there is no correlation of errors between two magnets, then from Eq. (17-24)

$$\langle xx^\dagger \rangle = R\langle xx^\dagger \rangle_0 R^\dagger + (A - RA_0)\langle mm^\dagger \rangle (A - RA_0)^\dagger$$

This equation expresses the resultant distribution in uncertainty upon leaving the magnet. This model for misalignment has been implemented in TRANSPORT. It enables one to introduce a displacement uncertainty δx, say of Q-10, and trace its effect through the system. The computer was used to generate tables of misalignment effects.

Alignment criteria

The two main concerns in establishing alignment tolerances on the system are related to apertures and momentum definition. In general, magnet apertures are kept small to reduce cost. This means that the uncertainty of the

reference axis must be kept small so that the beam will pass through all magnet apertures. A radial displacement of the reference axis at the slit corresponds to passing a different mean momentum through the slit; hence, the uncertainty of this quantity must be small enough to prevent significant deterioration in the momentum-defining ability of the system.

Using the alignment model discussed in a previous section, the effects on the horizontal and vertical aperture at any point due to any type of misalignment of any preceding magnet were computed. Starting with zero phase space (i.e., the reference trajectory only), a small misalignment uncertainty of a specified type, say δx, is introduced at magnet j. The resulting horizontal and vertical phase space at points $k > j$, i.e.,

$$(\sigma_{11}(k))^{1/2} \quad \text{and} \quad (\sigma_{33}(k))^{1/2}$$

are computed. These represent the uncertainty in the reference trajectory due to the alignment error. In this way the partial derivatives

$$H_{ijk} \equiv \frac{\partial[(\sigma_{11}(k))^{1/2}]}{\partial(\mathbf{m})_i} \qquad k > j,\ i = 1, 2, \ldots, 6$$

$$V_{ijk} \equiv \frac{\partial[(\sigma_{33}(k))^{1/2}]}{\partial(\mathbf{m})_i}$$

are approximated for each magnet j and are tabulated in Reference 6. The units are centimeters per mil and centimeters per milliradian for the displacement and rotation misalignment derivatives, respectively. The unit "mil" denotes 0.001 in. and was the convenient unit when actually aligning the magnets. With this detailed information available, sensible compromises between aperture sizes and alignment tolerance specifications were made at an early stage of BSY development.

A look at the values H_{ijk} and V_{ijk} for system A showed that the alignment requirements amount to controlling the vertical displacement of the beam at B-17 and the horizontal displacement at the slit. The significant alignment errors contributing to vertical displacement at B-17 are the vertical displacements of Q-10, Q-11, and Q-12, and rotations of bending magnets B-10 through B-17 and pulse magnets PM-1 through PM-5. Individual vertical uncertainties due to misalignments given in Table 17-3 added on an rms basis to the beam envelope at B-17 give an increased phase space which still passes through the usable aperture of ± 2.4 cm after this magnet. The significant alignments contributing to horizontal uncertainty at the slit are also given in Table 17-3. At the slit, the dispersion in the A system is $r_{16} = 6.3$ cm/percent momentum spread. Therefore, a momentum bite of $\pm 0.05\%$ will pass through a ± 0.32-cm slit. If this definition is to be reproducible to $\pm 0.02\%$ over long periods of time, then alignment errors must not shift the central trajectory in excess of $6.3 \times 0.02 \approx 0.13$ cm. Individual radial displacements due to the misalignments of Table 17-3 when added on an rms basis result in a displacement less than 0.13 cm. Other misalignments did not

Table 17-3 Tolerances controlling vertical uncertainty at B-17 and horizontal uncertainty at the slit

Quadrupoles	$\delta y \leq 5$ mils	$\delta x \leq 10$ mils
Bending magnets	$\theta z \leq 0.33$ mrad	$\delta z \leq 170$ mils
Pulsed magnets	$\theta z \leq 3$ mrad	

significantly affect these two criteria, i.e., their alignment derivatives were very small. For further discussion of alignment tolerances and alignment techniques, see Chapter 22.

17-4 Problems associated with transport of high-intensity beams (HAW)

Thermal effects

The high-intensity beams delivered by the accelerator posed severe problems to the designers of beam transport equipment. Direct impingement of the electron beam on solid materials results in rapid temperature rise and prompt damage due to thermal stress or melting (see Chapter 20). For example, a 600-kW, 20-GeV, 0.6-cm diameter beam resulting from 1.7-μsec long, 50-mA peak current electron pulses at 360 pulses/sec will cause a rise of 50°C/pulse at shower maximum in copper. A material having low thermal conductivity, high atomic number, or low melting point will sustain severe damage after only a few pulses. Consequently, the beam cannot be allowed to impinge directly on vacuum chamber components for more than a few pulses. The usual causes of accidental impingement are change in beam position, direction, or beam cross section at the end of the accelerator; incorrect setting of bending magnets; and incorrect setting of focusing magnets.

Although the energy spectrum from the accelerator is good, at high beam current there is a considerable intensity of off-energy electrons. These electrons are deflected into the walls of the vacuum chambers in and downbeam of bending magnets, and the equipment, therefore, has to be designated to withstand continuous bombardment by these electrons. These electrons create all the problems of a mis-steered high-intensity beam, though to a lesser degree.

Beam power is continuously absorbed in dumps, targets, slits, collimators, and protection collimators where the latter are located to intercept the off-energy electrons. Some beam energy is also unavoidably absorbed in vacuum chamber walls. When the power density exceeds about 1 W/in.^{2}, water cooling is required.

There were some fears that the high rates of energy deposition would give rise to shock waves which would cause fracture or spallation. Tests of aluminum samples have shown that this does not occur at the power levels expected in the electron beam. However, thermal fatigue due to temperature

cycling is a recognized cause of failure of materials. Some parts of the power absorbers may reach temperatures high enough to cause thermal fatigue within the useful lifetime of the equipment. Thin, water-cooled sections are used to reduce temperatures where high-energy deposition rates may occur.

The pulsed magnets require vacuum chambers of low electrical conductivity to minimize eddy current heating. Materials having a low electrical conductivity usually have a low thermal conductivity and are, therefore, subject to failure by thermal shock. These chambers must be protected from excessive heating. Also, nonconductive materials are subject to failure due to buildup of internal electrical charge when irradiated with charged particles.

Primary radiation

In addition to thermal effects, the electron beam can cause radiation change. Organic materials (vacuum gaskets, electrical insulation, electronic equipment, etc.) are very sensitive to radiation. For example, the epoxy material commonly used for magnet coil insulation will become brittle and develop cracks after absorbing about 10^{12} ergs/g—the epoxy[7] used in SLAC magnets will lose strength after absorbing about 10^{14} ergs/g; polyethylene and polystyrene cable insulation become brittle and crack at about 10^{11} ergs/g; Teflon, butadiene, and polyurethane insulation become embrittled at about 10^{10} ergs/g; Neoprene and rubber become embrittled at about 10^{9} ergs/g; semiconductors change their electrical characteristics significantly at 10^{6} to 10^{8} ergs/g. None of these materials can be used in the beam or in its immediate vicinity. Most of them cannot be used in regions where the beam is absorbed or lost unless they are suitably shielded.

Metals and ceramics are highly radiation resistant. Even direct impingement of the beam on thin sections of low-Z metals and ceramics will not cause radiation damage in reasonable lengths of time. Significant changes in properties do not occur until doses exceed 10^{18} ergs/g. For example, a 1-MW, 5–20-GeV, 0.6-cm diameter beam will deposit about 0.8 kW/cm^3, or 3×10^{9} ergs/g/sec at a depth of 4.5 cm in a block of aluminum.

Secondary radiation

Beam loss in the beam transport system causes intense radiation. Continuous beam losses occur at the slits, collimators, protection collimators located after magnets, and, of course, in dumps. DeStaebler[8] has estimated the integrated radiation exposure 10 ft from a shielded slit to be about 10^{10} ergs/g in 10 yr. This figure was confirmed by Neet,[9] whose tests also showed that the integrated radiation dosage inside the shielding would be as high as 10^{13} ergs/g in 10 yr. Thus, of the available organic materials, only the SLAC epoxy[7] can be used near places where beam is absorbed. Cables for magnets, instruments, switches, etc., must be fiberglass or mineral insulated; vacuum feedthroughs must be ceramic insulated. Since these solutions are expensive, it is desirable

to make a transition to more conventional insulation as close to the equipment as possible.

Conventional electrical and electronic equipment cannot survive for long periods of time in high radiation, so this equipment must be removed to a safe distance. This creates difficulties for electronic equipment where the signal level is very low.

Glass becomes brown and opaque after about 10^6 ergs/g, so viewing windows and lenses cannot be used in or near the beam.

Lubricating oils and greases harden when irradiated. In tests at SLAC,[10] a polyphenyl ether oil hardened at about 10^{12} ergs/g. Thus, equipment in high radiation areas can be lubricated if the proper lubricants are used. Dry lubricants have greater radiation resistance, but none of those investigated proved reliable. The usual problem was that continuous coverage could not be maintained.

Induced radioactivity

Material that absorbs beam will become radioactive. DeStaebler[11] has estimated the radiation levels in the vicinity of beam scrapers along the accelerator. For 5 kW of beam power absorbed in a scraper, he estimated saturation radiation levels of 2.2×10^3 mrem/hour from the concrete walls of the accelerator housing. Measurements have shown that these estimates are approximately correct. Shielding of the sources and addition of boron to the concrete are discussed by DeStaebler as possible methods of reducing radiation levels. Radioactivity will make access for modification and repair very difficult. Provision must be made for shielding radioactive equipment and for working at a distance. The air surrounding the beam transport will absorb some energy and will become radioactive. Fortunately, most of this activity is due to short-lived isotopes. It is thus possible to seal the housing in operation and to ventilate at shutdown, after a short decay period. Water that is used to absorb beam energy or to cool energy absorbers will become radioactive.[12] The ^{13}N, ^{15}O, ^{11}C, and ^{7}Be are produced by irradiation of ^{16}O. Tritium (^{3}H) will also be produced. The ^{13}N, ^{15}O, and ^{11}C have short half-lives, but ^{7}Be and ^{3}H activity will build up to high levels.

FORMATION OF CORROSIVE GASES. When air is irradiated, ozone and oxides of nitrogen are formed. In the presence of moisture, the nitrogen oxides will convert to nitric acid. The production of nitric acid can be estimated as follows: Reference 13 gives a production rate of one molecule of HNO_3 for each 35 eV absorbed. It is estimated that for a 600-kW beam, 3–20 W are absorbed in air in the BSY. Since 1 W equals 6.23×10^{18} eV/sec, 18×10^{16} HNO_3 molecules/W-sec are formed. For 20 W of power absorbed in air, 33 g of HNO_3 are produced each day. This is equivalent to about 0.06 liter/day of 35% concentrated acid. After 5 days of continuous operation, 165 g will have been produced, giving a concentration of about 6 parts per

million if evenly distributed throughout the switchyard housing. The greatest concentration of absorbed radiation will be in the vicinity of the high-power beam absorbers. It is difficult to predict whether the nitric acid will be uniformly distributed or will be concentrated near the energy absorbers. Continuous or frequent ventilation would reduce the concentration of nitric acid in the air, as would chemical scrubbing or chemical neutralization. Removal of water vapor from the air or exclusion of oxygen from the housing would reduce the production of nitric acid.

Very few materials are nitric acid-resistant, and most of these are expensive. Stainless steels, glass, ceramics, and high-silicon cast iron are very good at all concentrations of acid. Certain plastics such as phenolics, vinyls, and epoxies are fairly good at some levels. Plating is not very useful at high concentrations of acids. Very few plating materials are nitric acid-resistant (gold, chromium), and minute plating flaws can destroy the effectiveness of even these materials.

LIMITED ACCESS. During operation, radiation levels in the switchyard housing are so high that human occupancy is ruled out. Equipment must be designed to operate unattended. Beam instrumentation must be remote-reading and remotely operable. Personnel and equipment protection must be automatic.

After running at high-power levels, time must be allowed for decay of radioactive isotopes in the air and for subsequent ventilation. Thus, diagnosis and repair of equipment failures is very time-consuming, making high reliability a necessity. It is also very desirable to locate marginally reliable equipment and equipment requiring frequent adjustment or servicing in accessible areas.

After long periods of operation at high power, equipment in the vicinity of the beam will become radioactive. This will make modification and repair increasingly difficult. Equipment must be designed for quick adjustment and removal and for ultimate removal by personnel shielded from the high radiation. Again, high reliability and minimum maintenance must be incorporated into the design of all equipment.

Shielding

Shielding problems in the BSY are primarily of two kinds: (1) for primary and secondary radiation, and (2) for radioactivity. In operation, the shielding must be adequate to protect personnel from photon, neutron, and mu radiation produced when the primary electron beam is intercepted. Thick concrete walls and earth fill will stop the photons and neutrons. The neutrons will tend to "duct" out of even mazed or baffled openings, so provisions must be made for shielding all openings. The muons have a very long stopping distance (equivalent to 50 ft of steel for 25-GeV incident electrons), so that high-density shielding must be used where muons are produced close to inhabited areas.

Cooling water from energy absorbers will be highly radioactive during operation, so these water lines must be shielded. Equipment absorbing beam inside the BSY will become radioactive, so local shielding will be required to permit access for maintenance and modifications during shutdown.

17-5 Beam switchyard design (HAW)

The beam switchyard transport system is a permanent part of the accelerator. It was designed to provide reliability, precision, and flexibility under the severe conditions of operation described above. The arrangement of the beam switchyard and some of the components and subsystems unique to the beam switchyard will be described.

The BSY equipment is installed in a 1000-ft long concrete housing buried under 30 ft of earth. Figure 5-23 shows typical BSY housing cross sections. The housing walls are reinforced concrete. Sections around targets, dumps, slits, and collimators are boron-loaded to reduce activation by neutrons. The walls, floor, and ceiling are painted with white radiation-resistant paint. Normal access is limited to a large opening suitable for trucks and two smaller accessways suitable for personnel. These openings are shielded, locked, and interlocked during operation.

An underhung crane riding on rails suspended from the ceiling has access to all equipment. The crane runs the full length of each leg. In the section where the beams diverge, the rails are interlaced and a transfer bridge is provided to shift cranes from one leg to another. Steel rails for a future shielded car are laid above the shielding ledge. Up to 4 ft of shielding may be placed on the shielding ledge to protect cables and electronics in the upper level from radiation during operation and to protect personnel from radioactivity during shutdown. Large air exhaust ducts are located at the end of all beam runs at both levels, making it possible to admit air through the main accessway, which has a large filter door and to ventilate every part of the housing.

All beam transport equipment is located in the lower level. All vacuum, water, and electrical connections can be made from the upper level through holes in the shielding, if necessary.

The nominal beam height is 5 ft, 6 in. above the floor. All equipment is supported on adjustable stands. Provision is made for 6 in. of precise jack adjustment from the upper level. Greater adjustments require insertion and removal of spacers. Radiation-resistant materials were used in the design of equipment for the lower level. Magnets, stands, and other equipment, which are not in high-radiation areas and could not economically be made of stainless steel, are coated with epoxy paint. Carbon steel parts in high-radiation areas are coated with special radiation-resistant paint (see Chapter 20).

The primary subsystems and components of the BSY include the vacuum system, water systems, power distribution systems, magnets and power supplies, instrumentation and control, beam absorbers, and targets and stands of various types.

The system of vacuum chambers for the transport equipment is entirely inorganic. All chambers are aluminum or stainless steel weldments with the exception of the pulsed magnet vacuum chambers which are discussed below. The quickly replaceable vacuum parts use indium gaskets with a SLAC-designed coupling. Water cooling of the vacuum chamber is provided where beam heating is expected. The vacuum pumps and gages are located on top of the shielding fill for ease in servicing. The pumps are conventional oil diffusion pumps with refrigerated baffles and mechanical backing pumps. The accelerator vacuum system operating at 10^{-7} torr is separated from the switchyard vacuum of 10^{-4} torr by a differential pumping system including ion pumps, a refrigerated baffle at $-40°C$, and fast vacuum valves. Radiation-resistant fast valves and isolation valves are scattered throughout the switchyard to protect the accelerator vacuum and delicate BSY equipment and to minimize pump-down time.

Two types of water systems are required: magnet water systems and radioactive water systems for beam energy absorbers. The magnet water system is fabricated from copper and stainless steel. Headers in the upper level of the housing supply low conductivity water to individual pieces of equipment. Flexible copper hoses supply water to each piece of equipment in the lower level. A remotely disconnectable stainless steel pipe union is installed in each line to permit removal of equipment. Individual return lines are brought through the shielding to return headers on the outside of the beam switchyard structure. Flowmeters, flow switches, valves, and thermometers are located in each return line where they can be reached in operation. All heat exchangers, pumps, surge tanks, and controls are also outside the housing. Separate water systems are provided for the A-beam and the B-beam. In an emergency, either heat exchanger can be used with either beam; each heat exchanger can handle both beams.

The radioactive water systems are stainless steel with copper in some systems and aluminum in others. The heat exchangers, pumps, surge tanks, and instruments are outside the switchyard. The radioactive water system equipment is shielded to protect personnel from radiation due to radioactivity in the water during operation. Radiation levels of 110 R/hour have been measured inside this shielding during operation. The heat exchanger pad floor is so arranged that leakage of radioactive water will drain into the switchyard housing where it can be stored until it has "cooled" and can be disposed of. No provision was made initially to handle evolved gases. A hydrogen recombiner system has since been developed (see Chapter 20). Connection to equipment is by commercial couplings with metal gaskets. It was feared that radioactivity in the water would build up to levels which would make repairs and maintenance of water system equipment difficult or impossible. This has not proved to be so. The ^{7}Be is captured in the demineralizers which are shielded and can be safely disposed of.[14] Tritium levels can be kept low by periodic changes of water, the period depending on the power deposition. Other activities are short-lived.

Magnets are of conventional design but are manufactured to tight tolerances to maintain the uniformity required. Coils are potted in radiation-resistant, alumina-loaded epoxy.[7] Each coil is protected by overtemperature switches. Insulators in the magnet water circuits are alumina. Pulse-to-pulse switching is done by five 0.1° laminated-core pulsed magnets with 0.1° bending angles.[15] The power supplies for these magnets consist of capacitor banks charged by vacuum tube rectifier power supplies and discharged through SCR switches (see Chapter 19). Pulse-to-pulse steering is accomplished similarly using smaller magnets and power supplies. The pulsed magnets have ceramic vacuum chambers because even low conductivity metals such as stainless steel and Hastelloy overheat in the pulsing magnetic field. Some apprehension was felt about damage due to accumulation of stray electrons and attempts were made to obtain ceramics with increased electrical conductivity. The attempts were unsuccessful, and subsequent tests of $\frac{1}{4}$-in.-thick samples of alumina in an electron beam produced no failures by this mechanism although 1 W/cm^2 was absorbed. (Samples did fail due to thermal shock.) The alumina has a very low thermal conductivity and is subject to damage due to shock, so protection collimators in the equipment protection system (see Chapter 20) prevent the beam from striking the chamber walls, but low-energy electrons can be deflected around the collimators, heating the walls. Thermometers were installed to turn off the accelerator upon excessive temperature indication. The alumina chambers are oval in cross section with stainless steel bellows and flanges at each end. The transition from alumina to metal is via thin stainless steel cuffs brazed to alumina. The alumina has a proprietary conductive coating both inside and outside to prevent surface charge buildup.

The pulsed steering magnets have Hastelloy vacuum chambers. The maximum field intensity is lower than in the 0.1° pulsed magnets and the maximum temperature in the Hastelloy is acceptable.

The vacuum chambers in the precise bending magnets are 316L or 304L stainless steel especially selected for low permeability to minimize local distortion of the magnetic field.

All the power supplies for the beam switchyard magnets are located in the Data Assembly Building next to the control room for ready accessibility. Direct current cables run outside the shielding as far as possible, then through duct banks into the upper level of the housing. They are connected to radiation-resistant, fiberglass-insulated cables which run to the magnets in the lower level. A SLAC-developed remote power disconnect is used to hook up to the magnets. The power disconnects are protected by locked covers; it is necessary to shut off the power supply before this cover can be removed. Power supply disabling switches and warning lights are provided in the vicinity of each magnet.

The instrumentation and control cables are similarly run outside the shielding to a point near the associated instrument, and then through a duct bank into the upper level. The connection to the instruments in the lower level is made by mineral-insulated coaxial cable or fiberglass-insulated wire. Both

Cerenkov cells and zinc sulfide screens are used in the beam, so optics and TV cameras are required. Front surface mirror optics are used to avoid problems with darkening of glass due to radiation. Radiation-hardened TV cameras are very expensive, so cameras are shielded and easily replaceable. All beam line instruments are adjustable and removable from the upper level. Where electric motors are required, they are located above the shielding floor and are replaceable. Air actuators are metal-bellows sealed.

As mentioned above, the ceramic vacuum chambers are protected from the electron beam by protection collimators. Other vacuum chambers, instruments, etc., are similarly protected. Each protection collimator has an associated ionization chamber which is in the interlock chain and which serves to shut off the accelerator when the collimator is hit by the beam.

Beam instrumentation is provided to monitor beam position, beam current, and energy spread (see Chapter 19). The instruments read out in the Data Assembly Building where power supplies and controls are also located.

17-6 Early operating experience and design evaluation (EJS and JLH)

The first electron beam was delivered through the A-beam transport system and end station A to beam dump east on September 20, 1966. Since that date, numerous tests and experiments have been performed on the beam switchyard transport system. In addition, several preliminary experiments of a survey nature have been completed and others are in progress. In general, the operation of the system has been exceedingly satisfactory. The maximum electron energy to date is 20.16 GeV. A momentum spectrum of the electron beam obtained using the beam switchyard momentum analyzing system is shown in Fig. 8-17. The first positron beam was delivered to end station B on February 22, 1967. The maximum beam power which has been transported through the system is 240 kW. It is anticipated that the power level will soon be more than doubled. Multiple beams of various energies, currents, pulse lengths, and repetition rates are now routinely delivered to experimenters in the end stations. Electron beam spot sizes of 1 mm diameter have been achieved. Various early checks on the momentum calibration of the transport system have been made by comparing the A and B transport systems, by using a quantameter and Faraday cup, by comparing the end station spectrometer with the A transport system, and by calorimeter measurements. Although much more refined tests are required, the early tests indicate that the beam switchyard system satisfies the design criteria for momentum calibration and resolution given in Table 17-2. Early experimental studies of beam optics and beam isochronism indicate that the transport system behaves in agreement with the predictions of the SLAC TRANSPORT computer program, which was used to design the system. However, optics tests indicate that the transport system solid-angle acceptance is less than expected. This effect is not clearly understood, but is probably the result of misalignment of

components and certain known differences in the bending magnets of the system. Since the emittance phase space of the accelerator is much smaller than the achieved acceptance of the beam switchyard transport system, there is no difficulty in delivering the beam to the experimental areas.

Operating experience to date has emphasized the need for high reliability of equipment. Problems that hamper delivery of the beam are the usual ones of getting such a system to operate—e.g., interlock faults, power supply failures, slit drive failure, browning of TV camera lenses, vacuum failure, and personnel protection system failure. Since the initial turn-on, equipment has been damaged by the electron beam on two occasions: (1) a spring in a vacuum quick-disconnect valve was overheated, resulting in loss of elasticity and a vacuum leak, and (2) a vacuum quick-disconnect was overheated, causing the indium seal to melt, again resulting in a vacuum leak. At the power levels run to date, usually about 1 to 10 kW, no serious radiation or radioactivity problems have been encountered. The radioactivity induced in the radioactive water systems is already sufficient to restrict system ventilation during operation. Some of the cooling water becomes intensely radioactive, but most of the activity is short-lived (^{15}O, ^{11}C). The ^{7}Be is produced in the water and removed by the demineralizers. Demineralizers have been found to have about 100 μCi of activity when depleted. Equipment close to the beam is becoming radioactive, but remote operations have not yet been necessary. It is too early to evaluate the radiation resistance of special components.

Acknowledgments

The fundamental principles of the beam transport systems were proposed by K. L. Brown. The proposal was studied and recommended by S. Penner. R. Taylor was responsible for the development of the basic layout of all equipment and systems and for the basic criteria for all components. He was aided by many people in many areas: D. A. G. Neet, control and instrumentation; B. DeRaad (CERN), instrumentation and equipment protection; F. Bonaudi (CERN), general layout, services, and utilities; H. Brechna, magnets and radiation-resistant coil insulation; Bengt Hedin (CERN), magnets; Julius Muray, magnet instrumentation and pulsed power supplies; E. Garwin, vacuum, energy absorbers, and water systems; H. DeStaebler, radiation and radioactivity; H. Butler, beam optics and computer programming; S. Howry and C. Moore, computer programming; D. Coward, all areas; K. Trigger, alignment; A. Odian, parasitic gamma beam; D. Drickey, A photon beam; W. B. Johnson, physics (B-beam); R. Larsen, physics (B-beam); Z. Guiragossián, radiation and shielding; D. Fries, muon shielding.

The engineering of the switchyard was done under the direction of the *ad hoc* beam switchyard group. The contributions of support groups are acknowledged elsewhere. Beam switchyard group staff and their areas of responsibility were as follows: C. R. Johnson, equipment installation; C. A. Harris, power supplies; E. K. Johnson, electrical distribution and water;

E. Oster, magnets (this later became the responsibility of the Magnet Engineering Group under J. Gunn); L. Lucas, energy absorbers; D. A. G. Neet, instrumentation and control; J. Voss, supports and alignment; R. Allyn, mechanical engineering; R. Gould, plant engineering liaison; R. Pedersen and R. Short, technical planning liaison. Dorothy Ellison was group secretary during its entire lifetime.

References

1 K. L. Brown, "A First- and Second-Order Matrix Theory for the Design of Beam Transport Systems and Charged Particle Spectrometers," Rept. No. SLAC-75, Stanford Linear Accelerator Center, Stanford University, Stanford, California (July 1967).

2 S. Penner, *Rev. Sci. Instr.* **32**, 150 (1961).

3 C. H. Moore, S. K. Howry, and H. S. Butler, "TRANSPORT—A Computer Program for Designing Beam Transport Systems," Rept. No. SLAC-54, Stanford Linear Accelerator Center, Stanford University, Stanford, California (to be published).

4 R. Helm, "First- and Second-Order Beam Optics of a Curved, Inclined Magnetic Field Boundary in the Impulse Approximation," Rept. No. SLAC-24, Stanford Linear Accelerator Center, Stanford University, Stanford, California (November 1963).

5 S. Howry, "Second-Order Aberration Coefficients of a Quadrupole," Tech. Note, No. SLAC-TN-62-45, Stanford Linear Accelerator Center, Stanford University, Stanford, California (1962).

6 H. Butler, S. Howry, and C. Moore, "Specifications for the Beam Transport Systems to End Stations A and B," Rept. No. SLAC-29, Stanford Linear Accelerator Center, Stanford University, Stanford, California (1964).

7 H. Brechna, "Effect of Nuclear Radiation on Organic Materials; Specifically Magnet Insulations in High-Energy Accelerators," Rept. No. SLAC-40, Stanford Linear Accelerator Center, Stanford University, Stanford, California (1965).

8 H. DeStaebler, "Rough Estimates for Radiation inside the BSY When the Beam Is on," Tech. Note, SLAC-TN-63-69, Stanford Linear Accelerator Center, Stanford University, Stanford, California (1963).

9 D. A. G. Neet, "Radiation Exposure in the Switchyard," Tech. Note, SLAC-TN-65-9, Stanford Linear Accelerator Center, Stanford University, Stanford, California (1965).

10 D. R. Walz and E. J. Seppi, "Irradiation of Highly Radiation-Resistant Organic Lubricants and a High Temperature Paint," Tech. Note, SLAC-TN-67-13, Stanford Linear Accelerator Center, Stanford University, Stanford, California (1967).

11 H. DeStaebler, "Radiation Levels in the Vicinity of the Beam Scrapers," Tech. Note, SLAC-TN-64-23, Stanford Linear Accelerator Center, Stanford University, Stanford, California (March 1964).

12 H. DeStaebler, "Photon-Induced Residual Activity," Tech. Note No. SLAC-TN-63-92, Stanford Linear Accelerator Center, Stanford University, Stanford, California (1963).

13 S. C. Lind, C. J. Hochanadel, and J. A. Ghormley, *Radiation Chemistry of Gases*, Am. Chem. Soc. Monograph No. 151, Reinhold, New York, 1961.

14 R. McCall, "Activation of Water during Beam Tests," Tech. Note No. SLAC-TN-66-4, Stanford Linear Accelerator Center, Stanford University, Stanford, California (1966).

15 H. Brechna, "A Pulsed Bending Magnet for the Beam Switchyard Area of the Stanford Two-Mile Linear Electron Accelerator," Rept. No. SLAC-28, Stanford Linear Accelerator Center, Stanford University, Stanford, California (1964).

18

BEAM SWITCHYARD MAGNETS

H. Brechna, W. O. Brunk, A. W. Burfine, J. K. Cobb, Editor, D. R. Jensen, E. L. Oster, E. J. Seppi, and M. T. Stangenes

The purpose of this chapter is to describe the extensive system of magnets installed in the beam switchyard (BSY). Following a brief description of the overall system in which the major components are identified, a detailed discussion of the design, fabrication, and performance of each type of magnetic element is presented. Design parameters and costs are summarized in tables. The magnetic characteristics of the momentum-analyzing systems are described in the next section, together with a discussion of magnetic measurements and data reduction. Criteria used in selecting the location of each magnet are given, and the chapter ends with a comparison of three methods of setting magnet fields for momentum analysis.

18-1 Qualitative description of system elements (HB, WOB, ELO, MTS)

Each of the magnets in the beam switchyard transport systems is a discrete element performing a separate function. The most prominent magnets are the 3° bending magnets for momentum analysis and beam deflection and the 8-cm quadrupole magnets for beam focusing. These basic elements are used in both A and B systems of the BSY (see Fig. 17-1). In addition, there are five 0.1° pulsed deflection magnets used to switch the beam into system A or system B on a pulse-to-pulse basis, two 0.25° dc emergency deflection magnets which are used if the pulsed magnets fail, and two 18.6-cm quadrupoles used as field lenses at the symmetry positions in the two transport systems. Four dc magnets are used when it is required to deflect the A-beam down into a dump preceding end station A. In the B system, two 0.17° pulsed deflection magnets and a magnetic slit are used to select the destination of the beam in end station B on a pulse-to-pulse basis. The optical characteristics of the BSY are discussed in Chapter 17.

All of the momentum-analyzing magnets in the A and B beams of the BSY are identical in physical and magnetic characteristics except for relatively minor magnetic differences which will be discussed later in this chapter. These magnets are 3° bending magnets and are used in positions B-10, -11, -12, -13, -14, -15, -16, -17, -30, -32, -33, and -35 in the BSY. All of the quadrupole magnets used in doublets in the BSY are also identical in physical and magnetic characteristics. These magnets are located at positions Q-10, -11, -13, -14, -20, -21, -30, -31, -33, and -34. Continuing the catalog, the five 0.1° pulsed magnets PM-1, -2, -3, -4, -5, and the two 0.17° pulsed deflection magnets PM-30 and -31 are all the same, as are the dc emergency magnets B-1 and -2, the 18.6-cm symmetry quadrupoles Q-12 and -32, the pulsed steering magnets AP-1, -2, -3, and -4, the dump magnets B-23, -24, -25, and -26, the dc steering magnets A-10, -11, and -12, and the pulsed steering magnets AP-30 and -31. The remaining magnets in the BSY are all one of a kind. The most important magnets will be discussed in some detail, whereas the less critical ones will be dismissed with only a few words about general magnetic and physical characteristics.

Of all component groups in the BSY, the magnet and power supply system is predominantly the most expensive. Major considerations in the development of new types of magnet configurations were economy while still maintaining safety and reliability of operation. It was also essential that the magnet characteristics dictated by second-order beam optics be achieved. These included field homogeneity over a given area in the gap of bending magnets and constant field gradient over at least 90% of the aperture in focusing magnets. Design objectives of greatest concern were: (1) control of fringing field by shaping pole-piece ends; (2) achieving specified field homogeneity by pole shimming[1] in bending magnets; (3) optimization of core and coil sizes for the required dimensions of useful gaps and apertures; (4) suppression of dipole and higher-order multipole fields in quadrupoles[2]; (5) development of appropriate coil insulation to withstand integrated irradiation doses of 10^{11} to 10^{12} rad.[3]

In the case of the pulsed bending magnets, although specifications with regard to irradiation resistance and field homogeneity are essentially the same as in the dc magnets, a few additional factors are added. The pulsed magnets operate at a frequency of 360 pps, and fatigue problems over a period of at least 10 yr due to the effects of the oscillating magnetic field must be considered. The coils operate at a voltage of 2 to 3 kV with respect to ground and with approximately 1.0 kV between turns. They must, therefore, be insulated in such a way that no voids are left in the insulating material, because such voids could permit corona discharges leading to breakdown. As the conductor has to be of a multistranded water-cooled construction to prevent excessive eddy current losses, an impregnation process had to be developed which insured thorough penetration of the thermoset. In addition, of course, the insulating material had to have proven irradiation resistance. The vacuum chambers inside the pulsed magnet gaps are specially designed and constructed ceramic tubes, which withstand irradiation effects and do not crack

from charge accumulations. The use of metals or combinations of metallic and organic materials in the vacuum chambers had to be avoided because of eddy-current heating which would occur in the fluctuating, transverse magnetic fields.

With these special requirements, systematic development work was needed. Simple calculations based on known engineering practices and rough model magnet work were inadequate. A team effort was needed not only to design, build, and test prototypes, but also to enforce very stringent quality control to insure that all magnets of the same design would be closely identical. Uniformity of steel ladle analysis, mechanical tolerances, and quality of workmanship were closely scrutinized throughout the fabrication program.

General design consideration

The function of the BSY magnet system is threefold: (1) provision of bending forces to keep the particle moving in a predetermined path; (2) provision of focusing forces to restrict horizontal and vertical motion of electrons, so that they remain inside vacuum chambers of relatively small cross sections; and (3) provision of steering forces to compensate for the malfunction or misalignment of certain components and for residual magnetic fields.

The design of the BSY magnets was influenced by their interaction with the other components along the beam, such as control and monitoring systems, slits, and collimators.

All BSY magnets have iron cores which are very resistant to damage by radiation. Therefore the problem of irradiation resistance centered principally upon the choice of coil insulation material. When organic materials are irradiated, covalent bonds are broken by ionization causing displacement of atoms in the lattice structure. In electron machines the production of fast neutrons is approximately two orders of magnitude smaller than in proton machines of the same beam power, but the ionizing radiation fields are more intense. Therefore, standard organic materials cannot be used near beam absorbers. Since many magnets were to be located near beam absorbing units, a new coil insulation had to be developed.

The coil insulation is based on heat-treated and chemically treated glass fiber tapes as structural material and alumina-loaded thermosets as impregnants. The ratio of organic to inorganic materials in the composite insulation is low, yielding a surface distribution without too many detrimental changes in mechanical properties, reduced shear stress and adhesion to the conductor, and decreased hygroscopic absorption.

The final formulation which was used for interturn and ground insulation is

Thermoset: pure epoxies, 100 pbw (parts by weight).
Hardener: aromatic Amine, 3 pbw or Anhydride, 80 pbw.
Wetting agent: epoxy functional glycidoxylpropyl trimethoxy silane, 1–2 pbw.
Filler: pure granulous alumina with grain size 1–10 μ, 100–200 pbw.

Table 18-1 Design features of the beam switchyard magnets

Parameters	*Pulsed magnet*	*3° Bending magnet*	*8-cm quadrupole magnet*	*18.6-cm quadrupole magnet*	*3° dump magnet*	*Magnetic slit*	*Emergency magnet*
Beam energy (GeV)	25	25	25	25	25	20	25
Deflection angle (degs)	0.1	3	—	—	3	± 1.8	0.25
Combined units	5	Beam A: 4 + 4 Beam B: 2 + 2	Doublets	Singlet	4	1	2
Gap height (meters)	0.05	0.06027	—	—	0.076	0.0508	0.07
Aperture (meters)	—	—	$r = 0.04$	$r = 0.092$	—	—	—
Useful gap dimensions (meters)	—	—	$r = 0.037$	$X = \pm 0.1$ $Y = \pm 0.01$	—	—	—
Gap width (meters)	0.16	0.3	—	—	0.12–0.24	0.178	0.07
Flux density (T)	0.17	1.455	—	—	1.455	± 0.85	0.56
Field gradient (T meters^{-1})	—	—	7.5	4.33	—	—	—
Effective length (meters)	0.85	3.025	2	2	3	2.5	0.0648
Overall length (meters)	1.08	3.47	2.30	2.33	3.58	2.82	0.93
Field homogeneity	10^{-3} (over $x = \pm 4$ cm)	$\approx 10^{-4}$ ($x = \pm 4$ cm)	—	—	—	10^{-3} ($x = \pm 2.5$ cm)	10^{-3} ($x = \pm 4$ cm)
Gradient linearity (%)	—	—	0.1 ($r = \pm 3.7$ cm)	0.1 ($X = \pm 10$ cm) ($Y = \pm 1.$ cm)	—	—	—
Peak current (A)	300	800	850	550	1000	700	360
Current density (A cm^{-2})	346	552	2600	700	700	560	572
Turns per pole	24	48	6	29	48	26	49
Terminal voltage (V)	2500	75	65	75	80	42	20

All coils were vacuum impregnated and cured under pressure at temperatures between 100 and 180°C. The high radiation environment also made it necessary to eliminate organic materials including natural and synthetic rubber from the magnet water-cooling circuits. Stainless steel connectors were used, with ceramic sleeves where electrical insulation was needed.

The magnet core and poles consist of forged or rolled steel with the following impurity composition: C—0.12% maximum; total A + Mo + S + P—0.1% maximum; total Mn + Ni + Cr + Cu + Si—0.7% maximum.

Manufacturing tolerances (deviations from calculated contours) were kept within 0.0002 in. on straight pole surfaces, and 0.0025 in. on contoured surfaces. In general, gap errors obtained in manufacturing were a factor of 2 or 3 better than the specified tolerances.

All magnets except the steering magnets and photon beam magnets are equipped with magnetic mirrors which confine the fringing field area and define the effective magnetic length. To eliminate second-order effects on the beam due to iron saturation and fringing fields, the pole ends and pole contours are shimmed. With the exceptions noted, the above remarks apply to all BSY magnets. In the following sections, design and construction details of each of the main types of magnets will be given.

The pulsed magnet system

The pulsed magnet system is designed to deflect an electron or positron beam of momentum up to 25 GeV/c by 0.5° to either side of the central axis. The deflection is achieved on a pulse-to-pulse basis by a series of five identical pulsed magnets. The main features of these magnets are given in Table 18-1.[4]

The core was manufactured from 0.035-cm cold reduced, grain oriented, silicon steel laminations which were stamped to the required tolerances. Epoxy was applied to one surface of each lamination, and the laminations were stacked in a rigid fixture to form the core. The assembly was evacuated to approximately 1 torr, vacuum impregnated, and cured under a pressure of 0.2 to 0.5 kg-cm^{-2} at a temperature of 125°C. The core consists of two E-shaped parts, welded at the outside surfaces to structural channels and bolted rigidly to each other. A pulsed magnet with its magnetic mirror attached is shown in Fig. 18-1. The stainless steel water connections and the structural parts are clearly visible. The normalized induction integrated over the length ($\int B\,dz$) at the median plane, as a function of horizontal displacement x perpendicular to the beam axis, is given in Fig. 18-2.

Multistranded water-cooled cable was wrapped in medium-weave glass tape and the wound coil was spaced by means of small glass fiber blocks from the mold walls and bottom plate. The assembly was vacuum impregnated with alumina-loaded thermoset, and cast in a single operation. Great care had to be taken during impregnation, casting, and curing to prevent any voids and fissures in the insulation. As mentioned above, these could lead to corona discharges and thus to a total destruction of the coil.

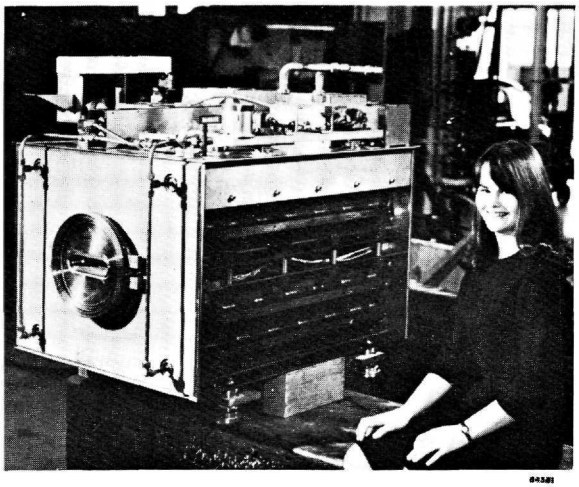

Figure 18-1 0.1° pulsed magnet.

Figure 18-2 Field plot of 0.1° pulsed magnet.

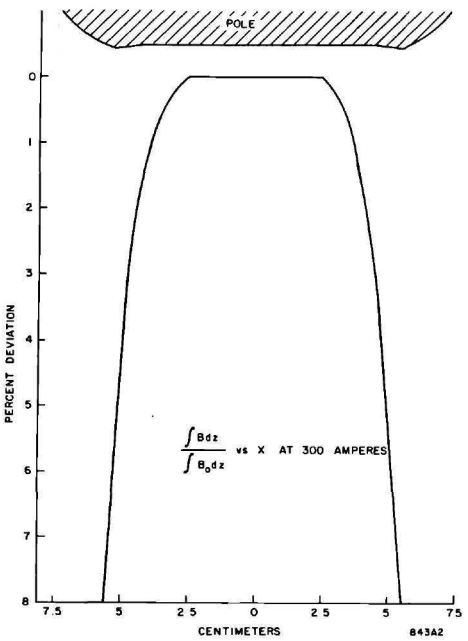

Prior to manufacturing the coils, a prototype coil was sectioned and tested for impregnation quality. The manufactured coils for all pulsed magnets were tested by means of a sensitive corona tester[5] and other nondestructive high-voltage methods to check for voids and poorly impregnated spots. A few details are worth mentioning. Stainless steel end plates providing compressive stress on the cores led to excessive induction heating and were eliminated at the pole ends. The thermoset between laminations provided adequate adhesion. The remainder of the end plates, the purpose of which was to keep the core under constant pressure, were not removed. Because of initial procurement difficulties with the ceramic vacuum chamber to be placed in the gap, the pulsed magnet cores were designed so that they could be sealed in a vacuum-tight envelope to permit the entire magnet assembly to be evacuated. This step became unnecessary as the ceramic chambers proved to be satisfactory as noted below. The ceramic vacuum chamber in the gap has an oval cross section with a height of 4.76 cm, a width of 17.5 cm, and wall thickness of 0.476 cm. It consists of 96% alumina and is coated with a low resistivity titanium compound inside and out. Welding the vacuum chambers to adapter flanges proved to be very difficult, but the job was finally completed successfully, using a heliarc welding technique.

In case of pulsed magnet failure, an emergency dc magnet is provided at each end of the row of pulsed magnets. The two emergency magnets are also capable of bending the beam 0.5° either side of the incident beam line. They are designed with 0.32-cm-thick laminations in order to permit the field polarity to be reversed within 2 sec. The emergency magnets are H-type with a gap height of 7 cm and a central field of 0.56 T.

The 3° bending magnets

Twelve of these magnets are used in the switchyard; two groups of four in the A-line bend the beam through 24°, and two groups of two in the B-line bend the beam there through 12°. For the purpose of design, the beam was assumed to have a diameter of 0.6 cm, a divergence of 10^{-4} rad, and a momentum spread of 2.6%. These figures are for the A-beam. The corresponding values are the same for the B side except a momentum width up to 5.2% is acceptable. Because of magnet resolution, the emergent beam would then be 4.8 cm wide at the exit of the magnet system. Such a beam was required to be deflected without appreciable loss in quality.

To conform with these requirements, the gap height was chosen to be 6 cm, and the pole ends in the x-y plane were shimmed to avoid saturation at operating fields of $B_{0,0,0} = 1.45$ T.[1,6] For the required homogeneity of $B_y/B_{0,0,0} = 10^{-4}$ over $x = \pm 4$ cm, the pole width was chosen to be 30 cm. A few of the most important design features are given in Table 18-1.

The main dimensions of the 3° bending magnet can be obtained from Fig. 18-3. Measured curves of B_y versus x at various z coordinates are given in Fig. 18-4. The deviation of B_y from $B_{0,0,0}$ at various excitation currents is

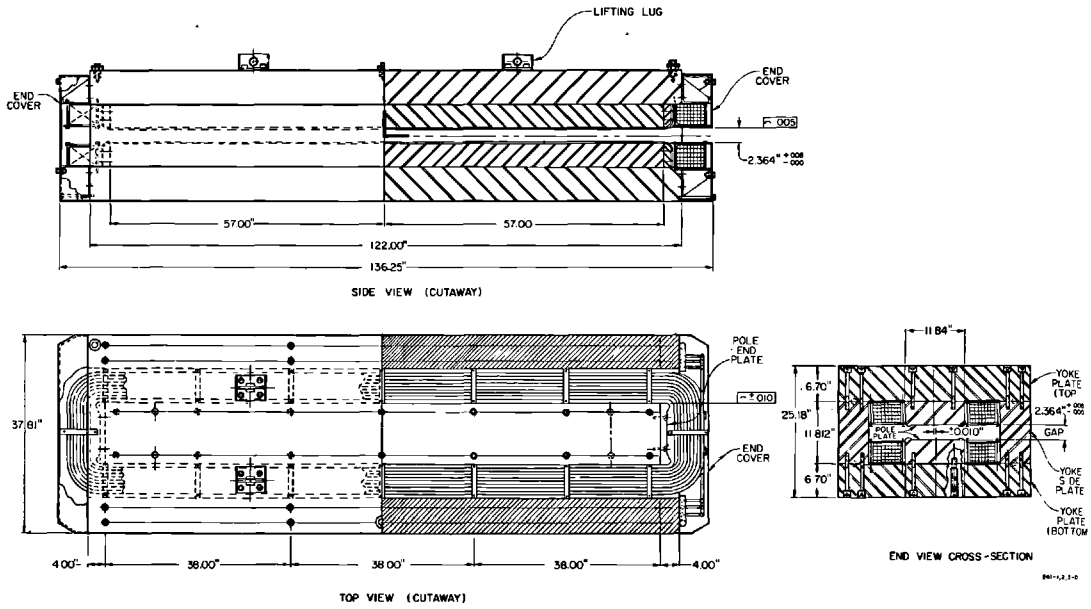

Figure 18-3 Diagram of 3° bending magnet.

Figure 18-4 Field plot of 3° bending magnet No. 7 at 800 A and at longitudinal positions measured from the center of magnet ($z = 0$, $x = 0$).

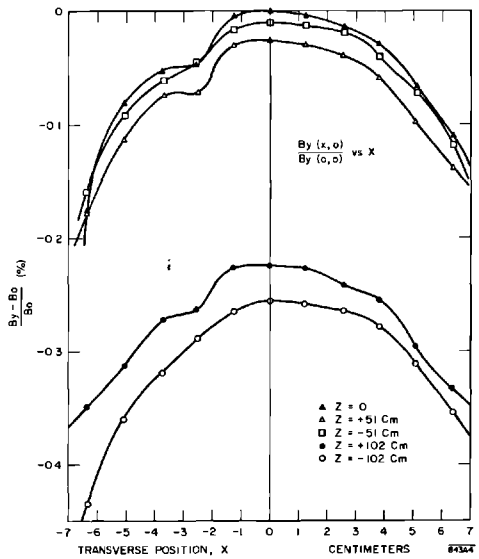

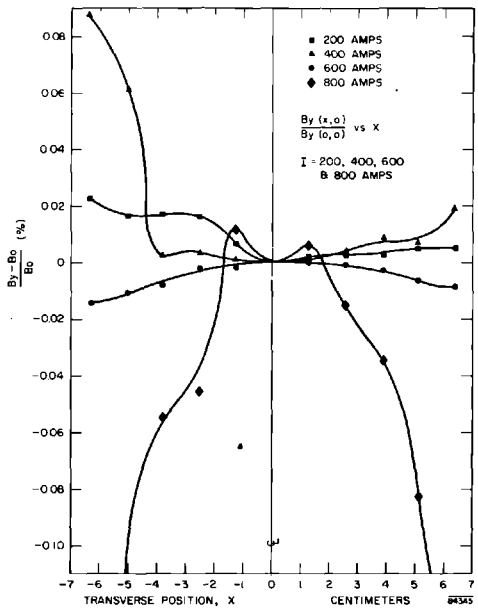

Figure 18-5 Field plot of 3° bending magnet No. 7 at various currents, one longitudinal position ($z = 0$).

given in Fig. 18-5. To prevent saturation effects at the entrance and exit of the magnet, the pole ends were circularly shaped with a radius equal to five-twelfths of the gap height. The magnet is provided with mirrors. For a given actual magnet length, the use of rounded pole ends leads to a somewhat shorter "effective length," but the field homogeneity in the gap is preserved over wider field ranges.

COIL CONSTRUCTION. The excitation coils consist of six double pancakes, each having sixteen turns. The hollow square-section copper conductor has an open-weave glass tape insulation which is treated with Volan-A and applied by a wet lay-up technique. This insulation method was necessary to ensure thorough wetting of the conductor surface. The insulation was applied as follows. The coil without ground insulation was placed in a mold with movable sides. The highly loaded thermoset was pulled through the insulation under a vacuum of ≈ 1 torr for 4 to 8 hours at about 40°C to guarantee uniform interturn impregnation. After this, mechanical pressure was applied through the movable mold walls onto all surfaces of the double pancake, and the assembly was given a primary 12-hour cure at 100°C. Unfortunately, a semicuring of the interturn impregnant was not possible due to manufacturing problems. Thus, prior to the application of the ground wrap the double pancake surfaces had to be cleaned and sandblasted. After the wet lay-up

of the ground insulation, the second impregnation was performed identically to the interturn impregnation. The insulation process was a delicate one, requiring skill, care, and close supervision to eliminate the inclusion of voids in the finished casting.

CORE STRUCTURE. The required gap-field homogeneity made it necessary for the core-iron to meet stringent specifications regarding impurity content, size and distribution of voids, and gas enclosures and fissures. Gap tolerances on the finished cores were required to be within 1.5×10^{-3} cm. Low-field measurements[7] also revealed that the silicon content had a significant influence upon the low-field behavior of the various magnets.

Owing to irradiation effects the pole surfaces were supposed to be nickel-plated to inhibit corrosion. However, due to lack of time, only an organic protective surface was utilized.

MAGNET ASSEMBLY. It was apparent that the air gap could not be reset to the specified close tolerances if the core had to be disassembled and reassembled to permit coil installation. For this reason, the coil supports were designed so as to allow insertion of coils and supports without disturbing the core steel assembly. Figure 18-6 illustrates a 3° bending magnet prior to installation in the BSY.

The 8-cm quadrupole magnet

In order to realize near-perfect focusing in quadrupole magnets, the field gradient in the central magnet region must be constant and the field shape at the entrance and exit of quadrupoles must follow a predetermined pattern.

Figure 18-6 Photo of 3° bending magnet—lead end.

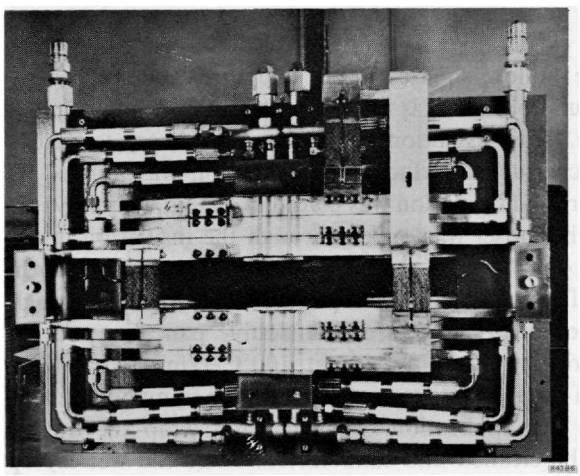

Excellent focusing is achieved if the field gradient along the z axis over the entire lens length and in the boundary region changes linearly with excitation and is practically zero at the mirrors.

In calculating the focusing properties of magnetic fields, a common approximation is to assume that the field is constant over the length of the magnet to virtual boundaries located a certain distance from each pole end.[8] In ordinary quadrupole magnets, the distance between virtual field boundaries, the effective length, changes with magnetic field intensity in a nonlinear fashion. This proves to be troublesome if the magnet must focus over a wide energy range. To compensate for this deficiency, the main design objectives for the BSY quadrupoles were: (1) to guarantee a constant gradient with a negligible harmonic content over 90% of the useful aperture area; (2) to make the "gradient-length product" change as a linear function of the excitation current. The first requirement was accomplished by using hyperbolic pole shapes and physically placing the excitation coils with respect to the poles in such a way that coil dipole effect in the useful aperture was negligible. The second requirement was met by using three-dimensional hyperbolic pole ends that satisfy the potential functions.

Let the coordinates X, Y be designated as the magnet axis and x, y as the pole symmetry axis.

The potential function inside the magnet ($x = R$) is given by

$$V_1 = k_1 XY \tag{18-1}$$

The pole ends are shaped as three-dimensional hyperbolas yielding a potential function

$$V_2 = k_2 XYz \tag{18-2}$$

At $\theta = 45°$ (pole symmetry axis), this potential function is written

$$V_2 = k_2 z \frac{x^2}{2} \tag{18-3}$$

Using the center of the mirror as the origin of a new coordinate system and designating $z = l_p$ as the distance of the point P (transition point from the constant pole aperture to the variable pole end aperture) results in

$$V_1|_p = V_2|_p = k_1 XY = k_1 \cdot \frac{x^2}{2} = k_2 \cdot l_p \cdot \frac{x^2}{2} \tag{18-4}$$

where R = aperture radius inside the magnet. Then

$$k_1 = k_2 \cdot l_p$$

Combining Eqs. (18-3) and (18-4) yields

$$x^2 = \frac{2V_2^2}{k_2 z} = \frac{2V_2 \cdot l_p}{k_1 \cdot z} \tag{18-5}$$

Differentiating Eq. (18-5) yields

$$\frac{dx}{dz} = -\frac{1}{2}\left(\frac{2V_2 \cdot l_p}{k_1}\right)^{1/2} \cdot z^{-3/2} = -\tan\alpha$$

Again, at the transition point $z = l_p$,

$$V_2 = V_1 = k_1 XY = k_1 \cdot \frac{R^2}{2} \tag{18-6}$$

we get

$$l_p = \frac{R}{2\tan\alpha} \tag{18-7}$$

where α is the angle between the tangents at the transition point P for $x = R$ and $x = x(z)$. The choice of α is governed by two considerations: (1) At the transition point the field disturbance should be tolerably small, and (2) to keep the length of the quadrupole to a minimum, the pole end should not extend too much in the z direction. A good initial guess is $\alpha = 8$ to 12°.

Combining Eqs. (18-6), (18-7), and (18-4), we get the equation for the pole-end contour at $X = Y = x/\sqrt{2}$:

$$zx^2 = \frac{R^3}{2\tan\alpha} \tag{18-8}$$

For a pole-end surface with

$$x = \sqrt{2}X = \sqrt{2}Y$$

we get

$$XYz = \frac{R^3}{4\tan\alpha} \tag{18-9}$$

The practical approach was to approximate the pole ends close to the excitation coil by a spherical dome, as illustrated in Fig. 18-7.

The magnet cores were manufactured from sixteen separate steel pieces, which gave the manufacturer more opportunity to salvage out-of-tolerance components, permitted greater flexibility during assembly, and saved machining time. As might be expected, this increased the quality control work appreciably. The hyperbolic pole-end shapes were manufactured by means of templets and computer-controlled milling machines. These pole ends were bolted to the main pole body.

Main features of the 8-cm quadrupole are given in Table 18-1. Measured field and gradient differences integrated over z as a function of θ are illustrated in Figs. 18-8a and b. The multiple field distribution parallel to the z axis at $x = y = a$, where a is the aperture radius, is given in Fig. 18-9.

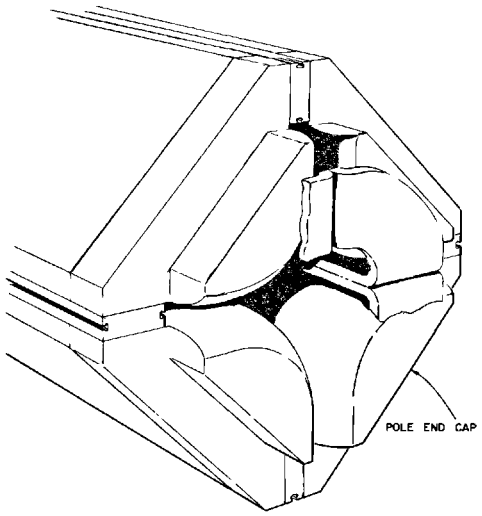

igure18-7 Poledetailsof 8-cmquadrupole iagnet.

'he 18.6-cm quadrupoles

'he main features of these lenses are generally the same as those of the smaller -cm quadrupoles, and the poles are shaped in the manner described above.)ne additional feature of the 18.6 cm-quadrupoles is the coil design. The urrent density distribution is such that the dipole component induced by the xcitation current is compensated so that it does not effect the useful aperture

igure 18-8a Field plot of 8-cm quadrupole No. 10.

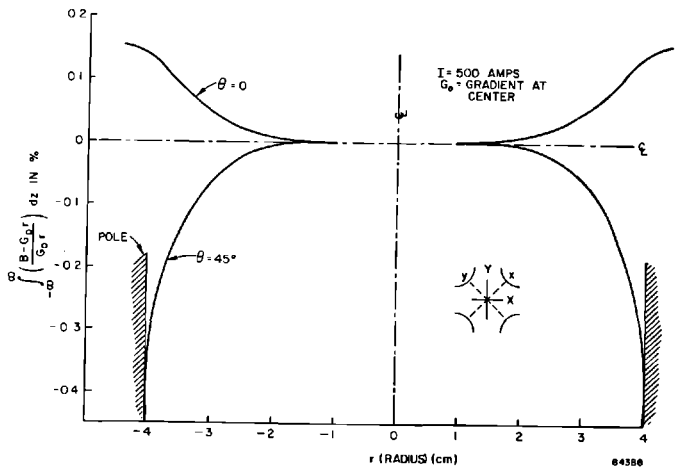

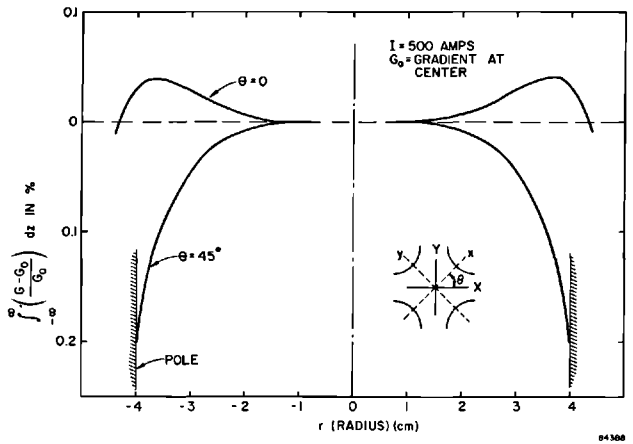

Figure 18-8b Gradient plot of 8-cm quadrupole No. 10.

area.[8] The cross sections of the coils for the large BSY magnets are shown in Fig. 18-10. Figure 18-10a shows how the current density of the coil in the region of the aperture for the 18.6-cm quadrupole is reduced by wider spacing of conductor.

The main design parameters of the magnet are given in Table 18-1. The coil and core designs are similar to those of the 8-cm quadrupole. The quadrupole front view is illustrated in Fig. 18-11, and Fig. 18-12 gives a typical fringing field plot at one end of the magnet.

Figure 18-9 Multipole content of 8-cm quadrupole No. 10.

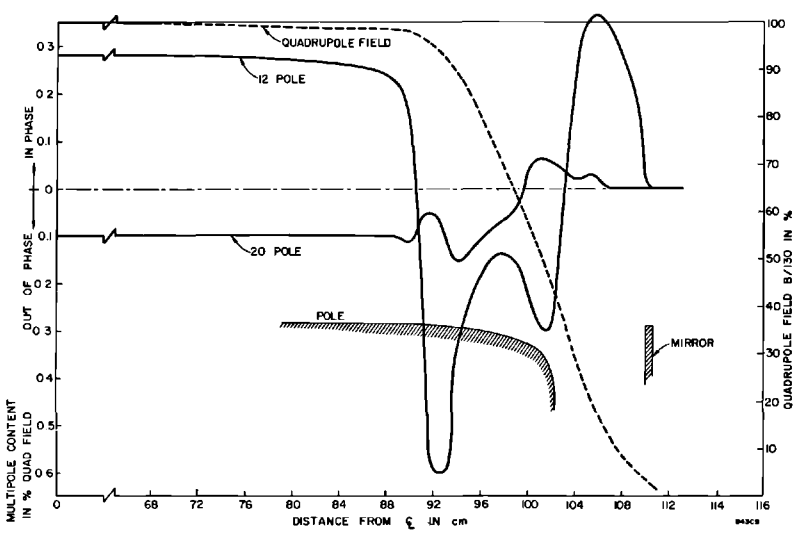

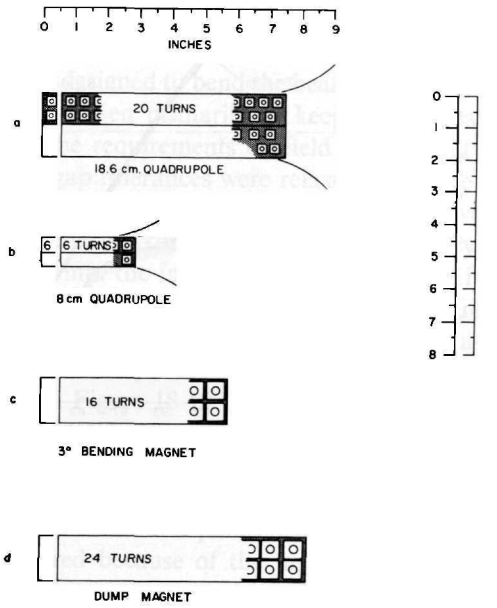

Figure 18-10 Some beam switchyard magnet coil sections.

Figure 18-11 Partial assembly of 18.6-cm quadrupole.

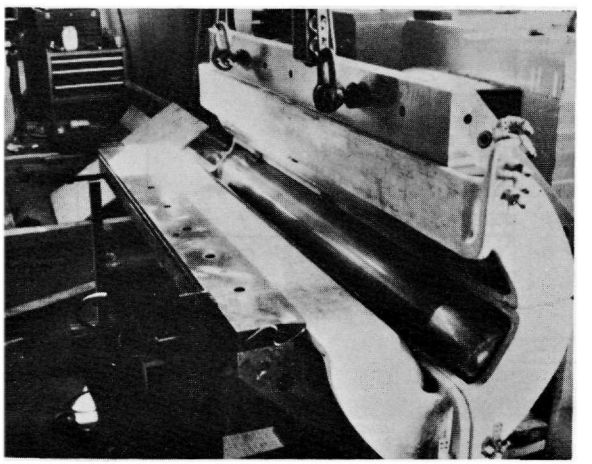

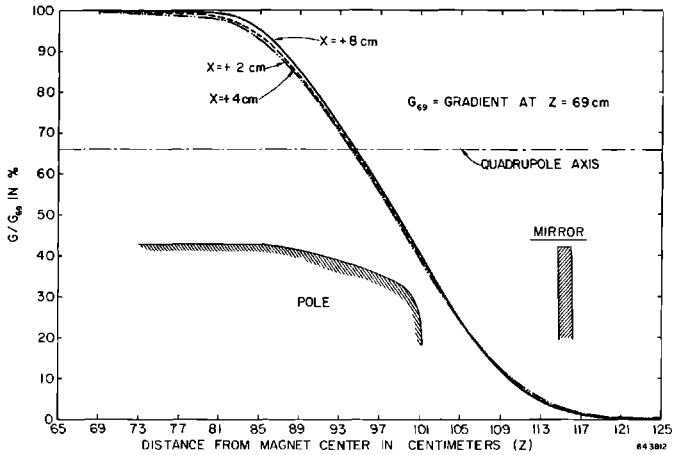

Figure 18-12 Gradient plot of 18-6-cm quadrupole at 600-A current.

Figure 18-13 Dump magnet.

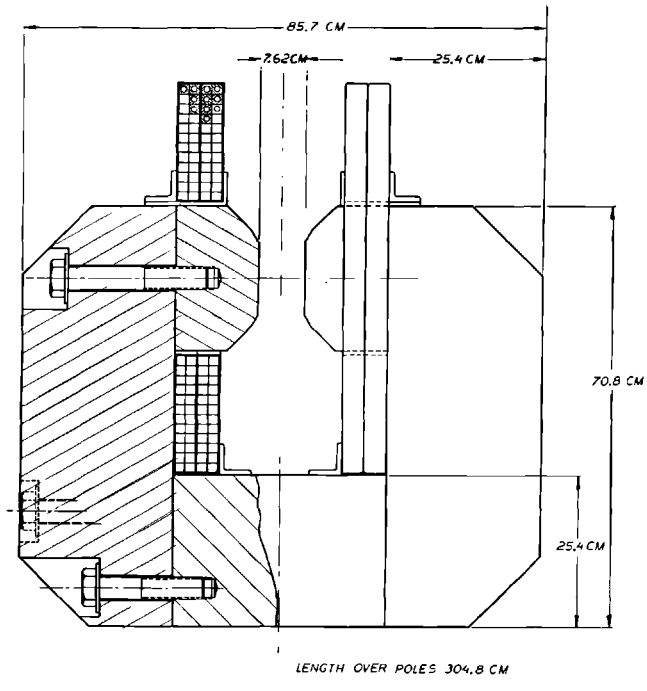

The dump magnets

The dump magnets are C-type magnets designed to bend the beam in a vertical plane. The C-type configuration was chosen primarily to keep the vertical plane free of obstacles on one side. The requirements on field homogeneity were not stringent and, therefore, the gap tolerances were relaxed. The poles are tapered and the yoke cross section is related to the pole area to achieve optimum flux distribution in the iron and maximum ampere-turn efficiency. As the magnet is close to the beam dump, the integrated irradiation dose is expected to exceed 10^{11} rad in a period of 10 yr. Coil and core designs are similar to those of the other BSY magnets. The interturn and ground insulations were applied using the wet lay-up technique described earlier. They were impregnated and cured simultaneously. Figure 18-13 is an assembly drawing of a dump magnet, and Table 18-1 gives the main design features.

The core material for these units was specified to be fully annealed plates of commercially available low-carbon (1010) steel.[9]

It may be pointed out that in most of the double pancake designs, counterflow heating problems were encountered because of the high thermal conductivity of the loaded thermoset used as interturn and interlayer insulation. In order to protect the coils against overheating, two thermoswitches were generally used for each hydraulic circuit. In the dump magnets one additional thermal switch, not anticipated in the initial design, was installed in each hydraulic circuit near the location of a hot spot discovered during test runs. Figure 18-14 shows a partially assembled dump magnet during magnetic field testing.

Figure 18-14 End view of dump magnet.

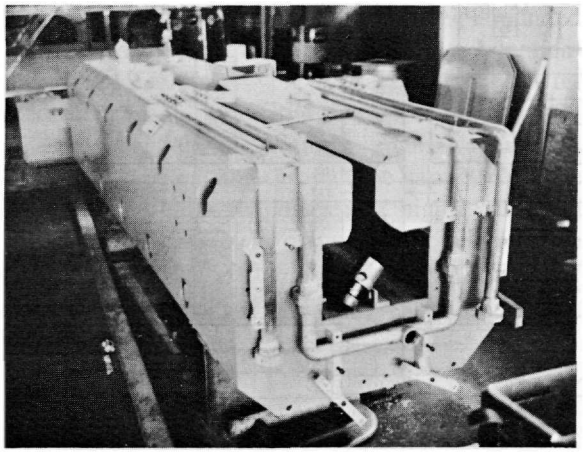

643413

The 2.5-meter magnetic slit

Near the output end of the B-beam transport system, a dc bending magnet (to be replaced in the near future by a pulsed magnet, similar to the 0.1° pulsed magnet) and a magnetic slit[10] are used to deflect the beam along any of three separate beam lines. The magnetic slit, essentially a combination of two C-type magnets separated by auxiliary poles and having a common gap (Fig. 18-15), is used to bend an initially deflected 20-GeV/c electron beam horizontally by an additional $\pm 1.8°$ or allow an initially undeflected beam to pass undeflected.

In the central part of the slit, a maximum field gradient of $\pm 3 \times 10^{-4}$ T/cm over a width of ± 1 cm was measured. The maximum field in the gaps

Figure 18-15 SLAC magnetic slit used in the beam switchyard.

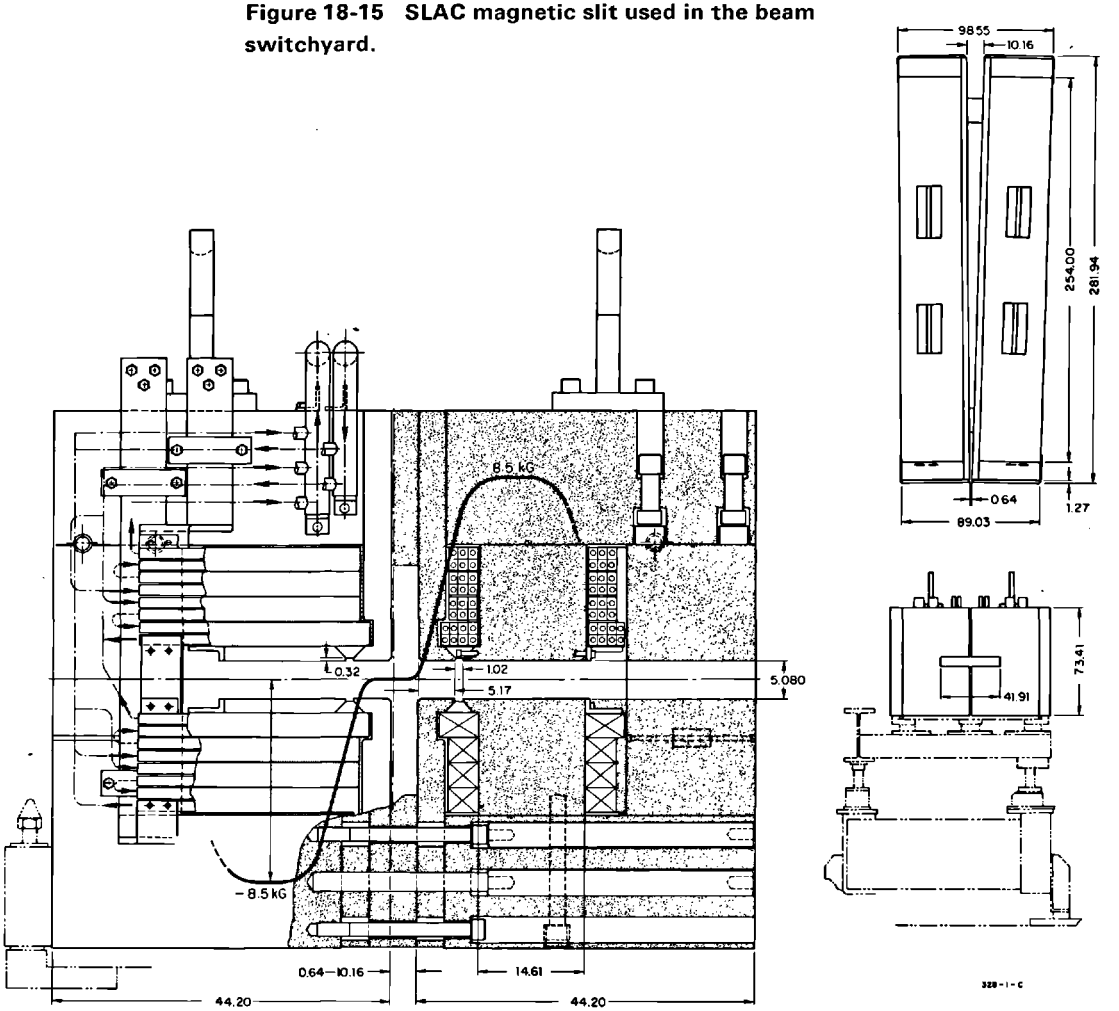

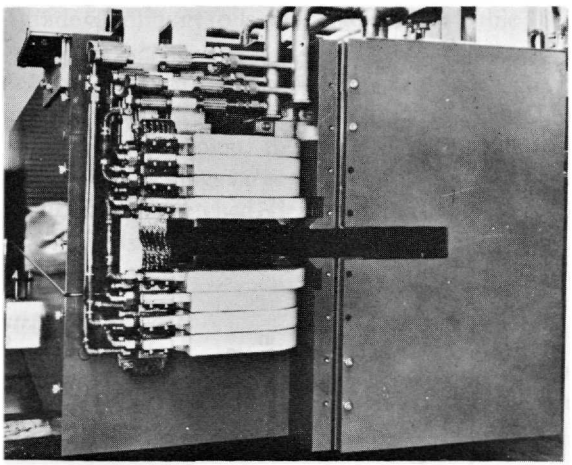

Figure 18-16 End view of magnetic slit magnet with one-half mirror removed.

is ± 0.85 T, corresponding to a beam deflection angle of $\pm 1.8°$. The gap area, where the beam is swept over $x = \pm 10$ cm, is free of obstacles and current sheets. The main features of the magnetic slit are given in Table 18-1. Figure 18-16 shows the 2.5-meter magnetic slit with part of the front mirror removed.

The pulsed steering magnets

These magnets are part of the common beam (prior to deflection into the A and B channels) and are used for beam steering on a pulse-to-pulse basis. Since the magnets are pulsed (600-cycle full sine wave, 360 pulses/sec maximum), the cores were built of 0.035-cm, grain-oriented silicon steel, laminated with Carlite insulation. The core dimensions are small and, thus, the laminations could be stamped as a single piece, simplifying the core assembly. After the laminations were stacked in proper fixtures, they were vacuum impregnated with a low-viscosity thermoset and cured. Mounting angles were welded to the outside core faces. The beam pipe passing through the gap should have a high electrical resistance to keep eddy-current losses low, high mechanical strength in order to keep the wall thickness down to a minimum, and must be able to be welded or brazed to stainless steel. After some searching, Hastelloy B proved to be the best choice. Table 18-2 illustrates the main features of the pulsed steering magnet.

The dc steering magnets

The magnets are used for horizontal and vertical steering in the A- and B-beam areas. The cores are manufactured of low-carbon (1010) steel plates.

Table 18-2 Main features of the beam switchyard pulsed and dc steering and photon beam stripping magnets

Parameters	*Pulsed steering magnets*		*dc steering magnets*			*Photon beam stripping magnets*	
	AP-1, ..., 4	PMV[a]	A-10, 11, 30, 31 400, 401	A-12	B-28	B-29	B-29A
Max. beam energy (GeV)	25	25	25	25	25	25	NA[b]
Deflection angle (deg)	0.0172	0.0143	0.0573	0.086	0.475	1.02	NA
Flux density in gap (T)	0.065	0.052	A-10, 11, 30, 31 0.33 A-400, 401 0.40	0.324	1.26	1.1	0.5
Effective length (meters)	0.384	0.405	0.254	0.266	0.38	1.09	1.09
Total length (meters)	0.482	0.482	0.365	0.362	0.622	1.37	1.37
Field uniformity (%)	0.1 ($x=\pm1.3$ cm)	0.1 ($x=\pm1.3$ cm)	0.25 ($x=\pm4$ cm)	1.0 ($x=\pm4$ cm)	0.6 ($x=\pm2.5$ cm)	1.0 ($x=\pm2.5$ cm)	1.0 ($x=\pm2.5$ cm)
Gap height (meters)	0.0388	0.052	A-10, 11, 30, 31, 8 cm; A-400, 401, 10.15 cm	0.127	0.0762	0.114	0.152
Gap width (meters)	0.127	0.1524	0.2014	0.203	0.1524	0.1524	0.170
Current (A)	21	23.8	25	36	500	850	850
Current density (A cm^{-2})	183	207	353	486	880	580	580
Turns per pole	48	48	462	462	104	158	132
Terminal voltage (V)	1340	1445	118	170	46	52.8	39.6
Weight (kg)	227	286	186	193	582	3110	2230

[a] Vertical pulsed magnet.
[b] Not applicable.

The coils are wound of EC grade aluminum foils and edge-cooled. Table 18-2 gives the main features of these magnets.

To compensate for the effect of the earth's magnetic field on the electron beam, two steering magnets with one single excitation coil made of aluminum foil were utilized. After curing the impregnant, the coils were machined to produce a saddle shape and provide openings large enough to pass the beam pipe through. The machined surfaces were etched, cleaned, and reimpregnated to prevent interturn shorts. The coils are air-cooled by natural convection.

Photon beam steering and stripping magnets

Three additional magnet elements are employed in the BSY magnet system as a part of the photon beam system. These units are of conventional design except for the use of radiation-resistant components.

Magnet costs

Table 18-3 gives a cost breakdown for engineering, coil and core procurement, and assembly for the major BSY magnets.

18-2 Magnetic characteristics of the momentum analyzing systems (JKC, DRJ, EJS)

To achieve the requirements for momentum calibration placed on the transport system, it was necessary to make magnetic measurements commensurate with a reproducibility of magnetic field setting of $\pm 0.02\%$ and an absolute field determination of $\pm 0.1\%$. Field distribution measurements were required to ensure that the magnet design achieved the field uniformity necessary to transport the beam without introducing significant aberration. Using the SLAC TRANSPORT[11] computer program, analysis of beam optics requirements indicated that $\int B(x, y, z)\, dz$ could vary no more than 3 parts in 10^4 for $-2.5 \leq x \leq 2.5$ cm, where B is the magnetic field in the magnet, x is measured in the traverse direction, y is measured perpendicular to the pole face, and z is measured along the longitudinal axis of the magnet. Another requirement placed on the transport system is that the direction of the beam leaving the system should be independent of particle momentum, i.e., the system should be achromatic.

Magnetic measurements (JKC, DRJ)

THE 3° BENDING MAGNETS. Magnetic measurements on the 3° bending magnets were performed in the laboratory. Later, they were repeated in the BSY with the magnets in final position and using the power and control systems provided for beam operations. The measurements were made using standard instruments; most were performed with a long-coil system. Two long coils

Table 18-3 Beam switchyard dc magnet procurement costs

Magnets	*Quantity*	*Core*	*Coil*	*Assembly*	*Hardware*	*Total*
3° Bending magnet	14	$165,479	—	$96,000 (incl. coils)	$30,000	$291,479
8-cm quadrupole	12	87,912	—	39,397 (incl. coils)	18,800	146,079
18.6-cm quadrupole	2	54,264	—	24,340 (incl. coils)	8,410	87,014
Dump magnets	4	—	$95,871 Total (coil, core assy.)		19,930	115,801
$\frac{1}{4}$° Emergency magnets	2	—	29,000 Total (coil, core assy.)		4,700	33,700
Magnetic slit	1	22,500	17,500	(In house)	1,510	41,510
DC steering magnets	7	2,500	3,632	(In house)	680	6,812

were used for measurements in the BSY. One of these is permanently located in the reference magnet, which will be discussed in Section 18-4 below, and the other was moved from magnet to magnet for comparison purposes.

The search coil consisted of a 3.75-meter long, epoxy–fiberglass coil form wound with copper wire. The coil rested in a cradle with roller supports at many points. The cradle in turn rested on the lower pole of the magnet being tested; it was adjusted so that the coil was in the central plane of the magnet. An electric motor rotated the coil upon command through slightly more than 180°. The coil output was fed into an integrating digital voltmeter which was set to integrate either positive or negative signals only. As the coil rotated, integration was inhibited until the coil plane was perpendicular to the direction of B. Integration then commenced and continued until the coil had rotated 180° and the output voltages had changed sign. This method required no accurately set limit stops on the coil flipping mechanism and improved the accuracy of the measurement. The long coils were periodically placed in 3° magnets with field profiles determined by direct measurements to check the coil constant. The readings of magnet excitation current were made with a 0.1 mohm, high-accuracy (0.02%) shunt in series with the magnet. The power supply run-up rate and current level were controlled by a stepping motor.

In order to make magnetic measurements reproducible, it was necessary to degauss the magnets before each test. It was found experimentally that the magnets could be consistently degaussed by the use of a reverse current held for some definite time and then decreased to zero. This technique of degaussing works very well if the magnet has been excited to at least 400 A. The reverse current necessary to degauss the magnet is dependent upon rate of change of current. A reverse current of 165 A held for 30 sec degausses all of the magnets to less than 0.5 G.

Long-coil measurements of two types were performed: (1) $\int B\,dz$ versus transverse position at several excitation currents I_{ex} and (2) $\int B\,dz$ versus I_{ex} at the center of the pole transversely and in the center plane. The measurements of $\int B\,dz$ versus I_{ex} were performed in 50-A increments and with two modes of current run-up, starting with a degaussed magnet. The modes were (a) "direct," in which the current is run up from zero current to the desired current with no intermediate steps, and (b) "incremental," in which the current is run up from zero to a current I_1, then to current I_2, etc., and a long-coil measurement is made at each current level. "Direct run-down" and "incremental run-down" measurements have also been made. In this case the measurements are made by decreasing the magnet current from an initial, well-defined magnetic state at 800 A. A 6-A/sec rate was chosen and, unless otherwise indicated, all measurements were made using that rate of excitation.

A typical graph of homogeneity of $\int B\,dz$ versus x is shown in Fig. 18-17. The dependence of run-up rate on the $\int B\,dz$ achieved for a given final current is shown in Fig. 18-18 for three different run-up rates. In Fig. 18-18 the line of zero deviation is the 6-A/sec rate, and it can be seen that the $\int B\,dz$ values for 9 A/sec are higher than the 6-A/sec values, while the 3-A/sec rate gives

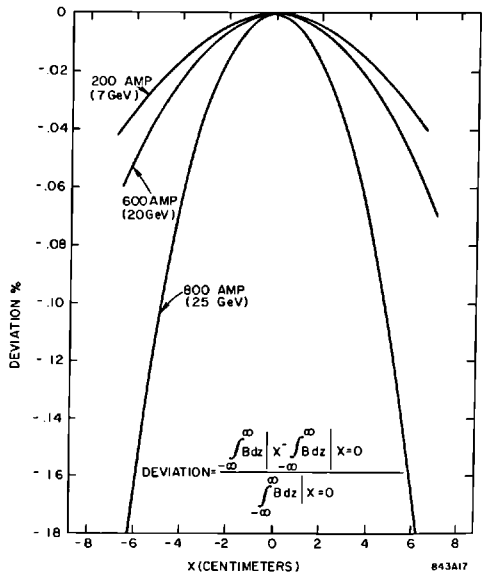

Figure 18-17 Field plot of 3° bending magnet.

lower values of $\int B\,dz$. This illustrates the need for using a single run-up rate. It has been mentioned before that measurements of B at a point in the magnet show a dependence on run-up rate which is different from that obtained for $\int B\,dz$. This can be seen by comparing Figs. 18-18 and 18-19. At other points in the magnet different B dependences are observed such that the integrated effect is consistent with that given by the long coil.

Figure 18-18 Average 3° bending magnet long coil measurements vs current.

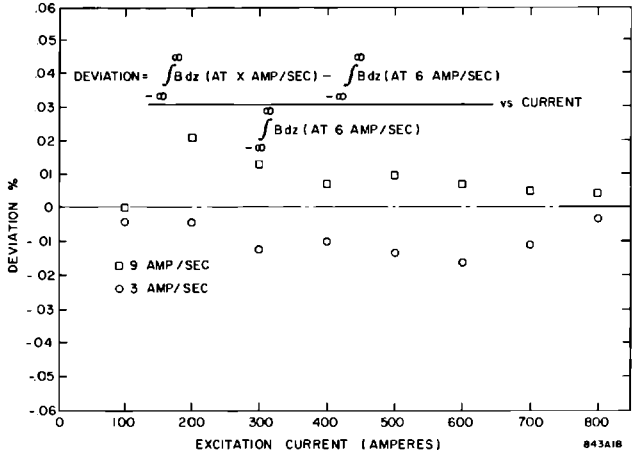

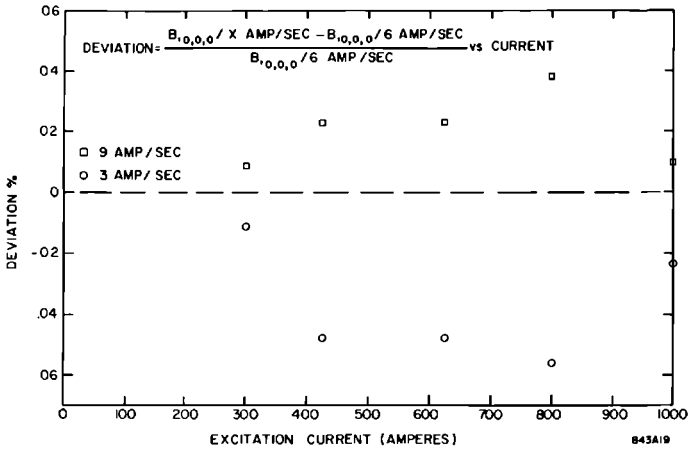

Figure 18-19 Average 3° bending magnet NMR measurements in center of magnet.

Differences of $\int B\,dz$ between magnets at a given I_{ex} can be attributed to differences in gap width, core length, and core impurities. Measurements of $\int B\,dz$ versus I_{ex} were made on each magnet, and it was found that the differences between magnets could be separated into two types: those that were current dependent and those that were not. The noncurrent-dependent differences were characterized by a nearly constant percentage offset of $\int B\,dz$ over the whole range of excitation current. The percentage offsets compared to magnet No. 4 are listed for each magnet in Table 18-4. Superposed on

Table 18-4 Summary of differences in $\int B\,DZ$ of magnets

Core No.	*Beam switchyard position*	$\frac{\langle \int B\,dz\ \text{Magnet}\ N \rangle}{\langle \int B\,dz\ \text{Magnet}\ 4 \rangle}$ *(in %)*
1	B-33	+0.347
2	A-ref	+0.193
3	B-10	−0.050
4	B-16	0
5	B-13	−0.020
6	B-12	+0.131
7	B-32	+0.015
8	B-11	+0.110
9	B-17	+0.120
10	B-ref.	−0.017
11	B-14	−0.049
12	B-15	−0.031
13	B-30	+0.084
14	B-35	+0.304

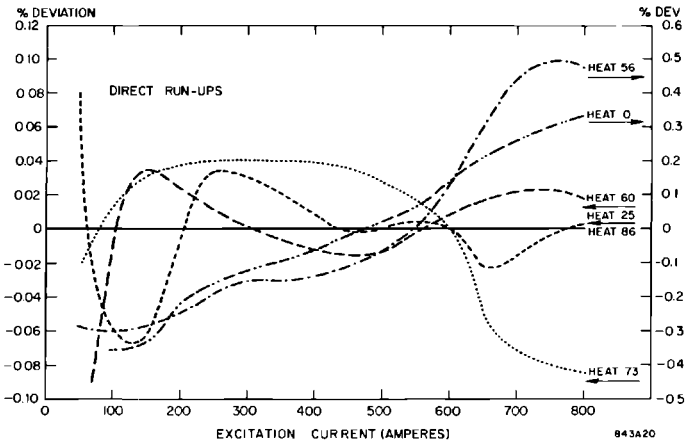

Figure 18-20 3° bending magnet—relative differences in $\int B\,dz$ caused by differences in steel impurities. Direct current run-ups.

these differences are current-dependent differences which group themselves according to the heat number of the steel from which the cores were fabricated. These differences, which are shown in Figs. 18-20 and 18-21, are seen to be quite large in the case of some heats. Figure 18-20 shows the relative differences attributable to steel impurities based on measurements of $\int B\,dz$ using direct run-up of current. Figure 18-21 shows similar data for incremental run-up of current. In these figures heat 86 is taken as the standard of

Figure 18-21 3° bending magnet—relative differences in $\int B\,dz$ caused by differences in steel impurities. Incremental current run-ups.

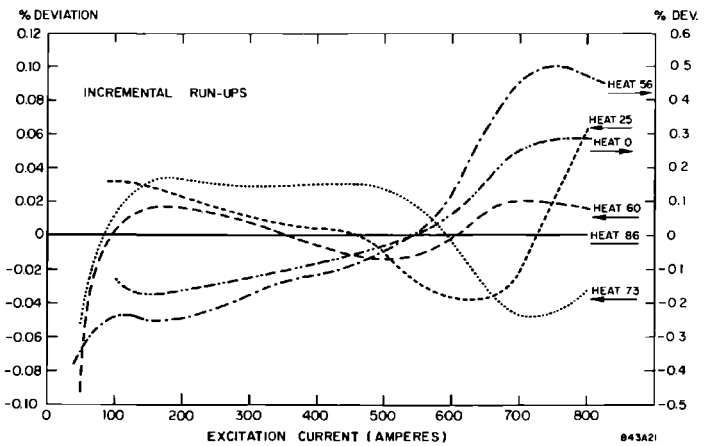

Table 18-5 Chemical ladle analysis, percent impurities in steel for 3° bending magnet cores

Impurity	*Heat No.* 56	60	86	0	73	25
C	0.06 %	0.06 %	0.06 %	0.05 %	0.08 %	0.07 %
Mn	0.29	0.26	0.30	0.15	0.28	0.30
P	0.009	0.009	0.008	<0.03	0.008	0.008
S	0.029	0.025	0.017	0.025	0.025	0.022
Si	0.004	0.18	0.18	0.08	0.13	0.16
Ni	0.02	0.01	0.04	0.06	0.04	0.01
Cr	0.03	0.05	0.04	0.01	0.04	0.03
Mo	—	0.01	0.01	0.01	0.02	0.01
Cu	0.05	0.04	0.04	0.04	0.04	0.03
Al	0.005	0.008	0.012	<0.005	0.009	0.004
Magnet Cores	1	2, 3 6, 8	4, 5 11	14	7, 9 10, 13	12

comparison and is plotted as zero deviation. Table 18-5 gives a chemical ladle analysis of the various heats of steel from which the magnet cores were made.

THE 8-CM AND 18.6-CM BSY QUADRUPOLES. The BSY quadrupoles were individually measured in the laboratory after assembly had been completed. Harmonic analysis was used to determine the deviation of B (r, z) from the ideal B expressed by G_0 $(0, z)r$, where G_0 is the field gradient at the magnet center. The nonlinearity of B integrated over the length was obtained by numerical integration of the nonlinearity of B over all values of z. It was found that the magnetic characteristics of all of the 8-cm quadrupoles were within the required tolerances of small aberrations for the size of the beam envelope at each position in the switchyard. The gradient length product versus the excitation current of each quadrupole was measured by a Hall probe gaussmeter using numerical integration of $B_r(r, z)$ over the length z to find the effective lengths and a Hall probe gaussmeter to find $B(r, 0)$ as a function of I_{ex}.

OTHER MAGNETS. All of the other magnets in the BSY were measured using long integrating coils to determine $\int B\,dz$ versus I_{ex} at $x = y = 0$ and $\int B\,dz$ versus x at several currents I_{ex}. The 0.1° pulsed magnets were also measured with a long coil, but instead of flipping the long coil the field was pulsed to obtain a measurement.

18-3 Reduction of data on beam switchyard magnets (JKC, AWB)

The 3° bending magnets

HYSTERESIS. The $\int B\,dz$ taken as a function of the excitation current I_{ex} was normalized to 50-A increments. The method used to normalize the data was a two-point linear interpolation using the points:

$$[(\textstyle\int B\,dz)_i, (I_{ex})_i] \quad i = 0, 1, \ldots, N$$

and

$$[(\textstyle\int B\,dz)_{i-1}, (I_{ex})_{i-1}]$$

with the assumption that $\int B\,dz|_{I_{ex}=0} = 0$.

This method was chosen in preference to a second- or third-order approximation because the difference between the normalized and unnormalized values was only several parts in 10^4.

A least-squares polynomial fit was made from the data points (both $\int B\,dz$ versus I_{ex} and I_{ex} versus $\int B\,dz$) on three different incremental run-up rates and on the direct run-up rate. From the polynomials, points were calculated using normalized current values and then compared with the data points. The parameters for the fit were as follows: decree—eighth; absolute error—2×10^{-4} (for a weight of 1.0); sum of errors—10^{-20}.

The calculated points were compared to bending magnet No. 4 (considered the standard magnet) for both direct and incremental run-up at a 6-A/sec run-up rate. Finally, the $\int B\,dz$ resulting from incremental current run-up was compared with $\int B\,dz$ resulting from the direct current run-up.

All data points were not given equal weight because less significant digits were obtained at low currents, and power supply regulation, current resolution, and $\int B\,dz$ resolution were also poor. The weights used for fitting were as follows:

50 A—0.1	200 A—0.6
100 A—0.2	250 A—0.9
150 A—0.4	$\geq$ 300 A—1.0

HOMOGENEITY. The parameters η and ε for each magnet were calculated from $\int B\,dz$ versus transverse position x, using the least-squares method where η and ε satisfy the equation

$$K = 1 + \eta x + \varepsilon x^2 \qquad (x \text{ in centimeters})$$

and K is defined by

$$K = \frac{\int B\,dz\,|\,x = x_n}{\int B\,dz\,|\,x = 0}$$

MOMENTUM ANALYZING SYSTEM. For a momentum analysis of the A-line series B-10, -11, -12, and -13, the beam displacement, momentum expected, and momentum obtained are given by the following equations. Let

$$A_I = \left[\frac{\sum_{m=1}^{N} \int_I B\, dz[m]}{N}\right]$$

The error (DX_I) is then,

$$DX_I = \sum_{J=1}^{N} \left[R[J] \sum_{K=1}^{J} \frac{(Y[\Sigma K, I] - A[\Sigma I]}{A[\Sigma I]}\right]$$

where

R = magnet displacement along beam line
J = magnet position
I = current level
$Y = \int B\, dz$

The measure of error is

$$E[I] = 1 + DX[I] \cdot 0.0015625$$

The expected momentum is

$$PE[I] = A(I) \cdot \frac{25}{4.3663374}$$

and the momentum obtained is

$$P[I] = PE(I) \cdot E(I)$$

In this calculation no correction was made for synchrotron radiation losses due to their very small magnitude. In the A-line the fractional energy loss in the bending magnets is about 1.6×10^{-4} and in the B-line the fractional energy loss is about 0.8×10^{-4} at 25 GeV.

THE 8-CM AND 18.6-CM QUADRUPOLES. From the measurements of $B_r(r, z)$ versus I_{ex} which were taken on the BSY quadrupoles the gradient $B_r/r = G_r$ was formed. The gradient versus I_{ex} was normalized to even current increments in the same manner as was done for the 3° bending magnets, and a least-squares polynomial fit was made from the data for gradient versus I_{ex} and I_{ex} versus gradient. The effective lengths were measured separately. The product of gradient and length was compared with the gradient length as calculated from TRANSPORT[11] and was used to determine the excitation current required to produce a given gradient–length product.

OTHER MAGNETS. The data taken from these magnets was normalized, and a least-squares fit was found for the polynomials $\int B\, dz$ vs I_{ez} and I_{ex} vs $\int B\, dz$ or $G_0 L$ vs I_{ex} and I_{ex} vs $G_0 L$ for quadrupoles. An eighth-order fit was used

for each of the magnets unless the computation was limited to a lower-order fit by the amount of memory available in the control computer used for setting magnet currents.

18-4 Selection of magnet location (EJS)

Initial TRANSPORT calculations made to design the BSY transport system assumed identical magnets, each bending the beam by 3°. However, in practice, the magnets are required to have identical current, and measurements show that small but significant differences exist in the $\int B\,dz$ magnetization versus current data for the individual magnets. (See Figs. 18-20 and 18-21 and Table 18-4.) The result is that the bending angle at each element in the system is not exactly 3° and, furthermore, the ratios of the various actual deflections produced by the magnets vary with current and, therefore, with the momentum setting of the system. Because the current through the system must be set to define the momentum, the exit angle from the system varies slightly with the momentum.

Because there were fourteen magnets to be assigned to fourteen positions, there were 14! ($\approx 8.7 \times 10^{10}$) possible permutations from which the optimum arrangement was selected. A number of magnetic features such as degaussing characteristics, transverse magnetic homogeneity, magnetization characteristics, etc., needed to be considered in determining the optimum permutation. However, measurements and calculations indicated that magnets were sufficiently identical that consideration of magnetic features other than magnetization was not necessary. The number of permutations was reduced significantly by imposing the requirements that momentum-defining magnets (the first four in A-beam and the first two in B-beam) and the respective reference magnets in each system have similar magnetization curves. This choice gives more confidence that future measurements on the reference magnets will indicate the behavior of the nearly inaccessible, momentum-defining magnets in the system. Also, since the requirements for optical quality are more stringent for high-energy experiments planned using the A-beam, this beam was given priority in the selection of the remaining magnets. Based on these requirements, the four magnets from heat 60, the magnets from the magnetically similar heat 86, and the magnet from heat 25 were assigned to A-beam. The magnetization data for these magnets and the heat-73 magnets was supplied to a computer program designed to select the permutation of magnet assignment which would result in a minimum deviation of the deflection of the exit beam from the ideal beam as the beam momentum was changed from one value to another. The program was required to select three magnets from heat 60 plus one magnet from heat 86 for the first four momentum-defining magnets. The remaining heat 60 magnet was assigned as the A-beam reference magnet. The last four magnets in A-beam were selected by the program from heats 86, 73, and 25, with the requirement that three

heat-73 magnets remain unused. This completed the assignment of magnets to the A-beam. The program was then used in a similar manner to assign the remaining magnets to location in the B-beam. Heat-73 magnets were used in the first two momentum-defining positions and as the B reference magnet. Table 18-5 gives the chemical ladle analysis for the steel from which the 3° bending magnet cores were made.

As a result of the magnet differences, the beam exit angle from the installed A-transport system varies from the design figure of 24.5° depending on the momentum setting of the system. If not compensated by the steering magnets provided at the end of the transport system, the extremes of angular variation for momentum settings between 3 and 20 GeV are sufficient to cause a motion of about 1 cm in the location of the beam spot in end station A. The corresponding displacement in end station B is about 4 cm.

18-5 Magnetic field setup for momentum analyses (EJS, JKC)

There are three methods of setting up the deflection magnets in the BSY transport system, two of which are presently in use and are being tested to determine their relative advantages. The first and operationally preferable method is to adjust the current in the deflecting magnets until the desired $\int B\,dz$ is achieved in the reference magnet. For this measurement, the long coil permanently installed in the reference magnet is used, and its integrating digital voltmeter measures the volt-second integration resulting from a flip of the coil. In this method, the $\int B\,dz$ of the reference magnet is related to the $\int B\,dz$ (and, hence, the momentum setting) of the transport system through the previous magnetic measurements on the individual magnets of the system. Obviously, this method requires that the $\int B\,dz$ in the transport system should track with the $\int B\,dz$ of the reference magnet. As has been discussed, magnets assigned to the momentum analysis locations of the transport system were chosen to have nearly identical $\int B\,dz$ magnetization variation with current. Tests have been performed to study the tracking characteristics of these magnets. It has been found that over the measured range of parameters, these magnets track each other to within 0.02%, independently of the run-up rate and the mode of operation (direct or incremental, up or down). Although the evidence is incomplete and further tests are planned, it seems that this method makes it possible to set up for a desired momentum analysis in a precise, quick, and flexible way.

The second method of setting the transport system to a specified momentum uses the current reading from a precision shunt in series with the transport magnets. The accuracy of this method depends upon the stability and accuracy of the current-monitoring shunt and associated voltmeter. This method requires that the magnets be degaussed and then set via direct run-up to the current corresponding to the desired momentum setting. This current setting is determined from analysis of the direct run-up magnetic measurements. To allow step increases in the momentum setting, tables giving the

required current change have been prepared from the incremental run-up measurements. These should give good results provided that increases in momentum of only a few steps are made and that the steps are not too large. All the tables were prepared by fitting eighth degree polynomials to the magnetic data. A similar scheme has been worked out using the run-down data. In using this method, the available data are only sufficient to allow changes in one direction during a single run. In principle this method for setting up the BSY momentum analysis system should be as accurate as the $\int B\,dz$ measurements outlined above. In particular, the direct run-up technique, although it is long and tedious, is based on a well-defined sequence on the hysteresis loop of the magnets. It should yield reliable results when a check on other methods is necessary.

A third method for establishing fields in the transport system magnets is based on readings from nuclear magnetic resonance (NMR) probes which are installed in the gap of each of the momentum-defining magnets. These probes give the induction at that point in the magnet. They can be used to set up the required magnetic fields for the deflection systems, but the accuracy is not as good as the long flip-coil measurements because the induction is sensitive to local variations in field and to gap changes caused by temperature variation. The installed NMR's, however, serve as a basic check against shunt changes or electrical shorts in the magnets and may detect anomalous behavior of a magnet which would not be reflected in the reference magnet readings.

Acknowledgments

The contributors to the work discussed in this chapter are many and all could not possibly be mentioned here but several deserve special mention. The overall criteria and basic calculations for a great part of the beam switchyard magnets were furnished by R. Taylor and by B. deRaad who is now at CERN. The design of the beam switchyard 3° bending magnets was a contribution of B. Hedin who also is now at CERN. The measurements program was initiated by J. Murray. G. Loew, R. Miller, and W. Herrmannsfeldt assisted greatly by contributing valuable advice during many hours of discussion.

References

1 B. Hedin, "A Bending Magnet with Nonsaturating Shimming," Rept. No. SLAC-19, Stanford Linear Accelerator Center, Stanford University, Stanford, California (September 1963).

2 J. Cobb and R. Cole, "Spectroscopy of Quadrupole Magnets" in *Proc. Intern. Symposium on Magnet Technol., Stanford Linear Accelerator Center, September 1965* (H. Brechna and H. S. Gordon, eds.), CONF-650922, p. 431, Clearinghouse for Federal Scientific and Technical Information, Springfield, Virginia.

3 H. Brechna, "Effect of Nuclear Radiation on Organic Materials; Specifically Magnet Insulations in High Energy Accelerators," Rept. No. SLAC-40, Stanford Linear Accelerator Center, Stanford University, Stanford, California (March 1956).

4 H. Brechna, "A Pulsed Bending Magnet for the Beam Switchyard Area of the Stanford Two-Mile Linear Electron Accelerator," Rept. No. SLAC-28, Stanford Linear Accelerator Center, Stanford University, Stanford, California (May 1964).

5 H. Brechna and E. Oster, "Insulation Structure and Coil Reliability," in *Proc. Intern. Symposium on Magnet Technol., Stanford Linear Accelerator Center, September 1965* (H. Brechna and H. S. Gordon, eds.), CONF-650922, p. 313, Clearinghouse for Federal Scientific and Technical Information, Springfield, Virginia.

6 J. K. Cobb, "The Prototype BSY 3° Bending Magnet," Tech. Note No. SLAC-TN-56-20, Stanford Linear Accelerator Center, Stanford University, Stanford, California (March 1965).

7 E. J. Seppi, J. K. Cobb, and D. R. Jensen, *IEEE Trans. Nucl. Sci.* **NS-14**, No. 3, p. 473 (June 1967).

8 H. A. Enge, *Rev. Sci. Instr.* **35**, 278 (1964).

9 H. Brechna, "Electromagnets for High Energy Physics Applications," in *Proc. Intern. Symposium on Magnet Technol., Stanford Linear Accelerator Center, September 1965* (H. Brechna and H. S. Gordon, eds.), CONF-650922, p. 1, Clearinghouse for Federal Scientific and Technical Information, Springfield, Virginia.

0 H. Brechna and J. Cobb, *Rev. Sci. Instr.* **38**, (9), 1289 (September 1967).

1 H. S. Butler, S. K. Howry, and C. H. Moore, "Specifications for the Beam Transport Systems to End Stations A and B," Rept. No. SLAC-29, Stanford Linear Accelerator Center, Stanford University, Stanford, California (June 1964).